AN ABSTRACT OF THE THESIS OF

RAYNOR YOICHI SHIMODA (Name) for the DOCTOR OF PHILOSOPHY (Degree)

in Electrical and Computer Engineering (Major) presented on May 2, 1973 (Date)

Title: Investigation of Electrical Field-Induced Optical Absorption Changes in CdS

Abstract approved: Redacted for privacy

Cheng C. Chang

The feasibility of using the Franz-Keldysh effect in practical light intensity controlling devices was investigated.

Reverse-biased diodes made from CdS were implemented to obtain high electric fields necessary for the effect. The three types of diodes studies were: MIS, metal-semiconductor barrier, and p^+-n heterojunction. An expression for the change in transmitted light intensities of the devices was derived in terms of the maximum electric fields in the space-charge regions. This expression was used to generate the calculated curves.

The changes in optical transmission spectra under the influence of applied voltages for both polarized and unpolarized incident light were presented. Changes in optical transmission of the order of one percent were observed for applied maximum electric field of 5×10^4 V/cm. Qualitative and quantitative comparisons of experimental results with theoretical predictions were made.

With the present technology, the maximum electric field the devices could withstand was approximately 10^5 V/cm. Several suggestions were made for possible improvement in the breakdown voltages of the devices.

Investigation of Electric Field-Induced Optical Absorption Changes in CdS

by

Raynor Yoichi Shimoda

A THESIS

submitted to

Oregon State University

in partial fulfillment of
the requirements for the
degree of

Doctor of Philosophy

June 1973

APPROVED:

Redacted for privacy

Assistant Professor of Electrical and Computer Engineering

in charge of major

Redacted for privacy

Head of Department of Electrical and Computer Engineering

Redacted for privacy

Dean of Graduate School

Date thesis is presented May 2, 1973

Typed by Karen Fincher for Raynor Yoichi Shimoda

ACKNOWLEDGEMENTS

It is a pleasure to express my gratitude to the many people who assisted and advised me in this work. Particular thanks go to Professor C. C. Chang of the Department of Electrical and Computer Engineering for his guidance during the course of this work; to the members of my committee who were instrumental in my arrival at this point in my career; to Dr. Jick Yee and Dr. Edmund Hsieh for their valuable contributions; to my wife for her understanding and constant encouragement and; to Mrs. Karen Fincher whose fast and efficient typing allowed me to meet the deadlines.

TABLE OF CONTENTS

LIST OF FIGURES

INVESTIGATION OF ELECTRIC FIELD-INDUCED OPTICAL ABSORPTION CHANGES IN CdS

I. INTRODUCTION

The theory of electric field-induced absorption changes in a semiconductor or insulator was introduced by W. Franz (9) and L. Keldysh (21). According to the theory, the optical absorption edge of a material shifts to lower energies when a uniform field of the order of 10^5 to 10^6 V/cm is applied. This change in absorption occurs only within a narrow region below the band edge (< 100 Å).

Since the appearance of the original papers, extensive work has been done in which experimental results are compared with theoretical predictions (10,16,22,35) and in which the effective masses (15) are determined. However, very little work has been reported on the possibility of applying the effect in the construction of practical devices. The theoretical predictions, i.e., large changes in transmitted light intensities over a relatively narrow region, make this effect very desirable in light valves. Uses of this voltage-controlled light valve would include electronic windows, optical circuit control and variable intensity filters.

The purpose of this project then is to design and fabricate devices which utilize the Franz-Keldysh effect. The characteristics of these devices are to be investigated and thereby their feasibility as practical devices are to be determined. The problems involved are also of interest.

After a brief review of the theory of the Franz-Keldysh effect and a study of the variables involved in the expressions for the change in absorption coefficient, we determined the desirable properties of the material. Equipment considerations also was a factor in deciding upon CdS as the semiconductor material.

Reverse-biased diodes were employed to obtain the necessary values of electric fields with relatively low applied voltages (< 20 volts). Three diode configurations, MIS, metal-semiconductor barrier and p-n heterojunction were used and their characteristics compared.

In order to compare these experimental results with our expectations, curves were derived which were in terms of the maximum electric field in the space charge region. The analysis used in arriving at the calculated curves is similar to Frova (11). Comparison of the calculated spectra with the observed spectra was done for the metal-semiconductor and p-n heterojunction diodes. The difficulties encountered in obtaining a good match were revealed.

Even with our limited resources and time we illustrated that the application of field induced absorption as light valves is feasible provided devices could be fabricated to withstand high electric fields; large reverse breakdown voltages in the case of diodes.

II. HISTORICAL BACKGROUND

The purpose of this chapter is to briefly summarize the pertinent work that has been done on both the theoretical and experimental aspects of the electric-field induced absorption in semiconductors and insulators.

The calculated change in absorption coefficient for both the ideal edge, i.e. $\alpha \sim (\hbar\omega-\varepsilon_0)^{1/2}$ and the exponential edge, i.e. $\alpha \sim \exp[\lambda'(\omega-\omega_0)]$ are presented in order to illustrate the complexity of the expressions.

The experimental results of previous work are mainly those treating cadmium sulfide material since our work will be with this material. The previous work indicates that the application of this effect should prove fruitful.

Theoretical Predictions of Field-Induced Absorption

The first calculations of the effect on the electric field on the optical properties of a crystal were done independently by Keldysh and Franz in 1958. Both workers treated only the fundamental edge absorption properties. The presence of the field results in a modification of the unperturbed square-root behavior and an additional absorption at energies $\hbar\omega < \hbar\omega_0$ which is essentially proportional to

$$\exp\left(\frac{\omega-\omega_0}{\omega_E}\right)^{3/2} \tag{2.1}$$

where $\omega_E^3 = \frac{e^2E^2}{12m^*\hbar}$

ω_o is the energy gap of the semiconductor

E is the electric field and

m^* is the reduced mass.

This gives thus an exponential-type tail in the long-wavelength region with a magnitude increasing exponentially with the applied field.

Franz derived an integral representation of the absorption coefficient in the presence of a uniform field which was valid both above and below the threshold energy. He evaluated this numerically and obtained oscillations of the absorption coefficient about the zero-field value for energies above the threshold (see Figure 1). He also considered absorption edges which are already of an exponential character without field, i.e., where the inherent frequency dependence is obscured by other absorption processes. In this case where the zero-field absorption

$$\alpha \sim \exp \lambda' (\omega-\omega_o) \text{ for } \omega < \omega_o$$

the expression for absorption as a function of electric field is given by (9),

$$A(\omega) \sim 1/2 \sqrt{\frac{\pi}{\lambda'}} \exp [\lambda'^3\omega_E^3 + \lambda' (\omega-\omega_o)] \qquad (2.2)$$

$$- \lambda'\omega_E^{3/2} \sum_{n=0}^{\infty} \frac{1}{3n!} \left(\frac{\omega-\omega_o}{\omega_E}\right)^n \sum_{\ell=o}^{\infty} \frac{\Gamma(3/2)(\lambda'\omega_E)^\ell}{\Gamma(3/2+[\ell-n]/3)}$$

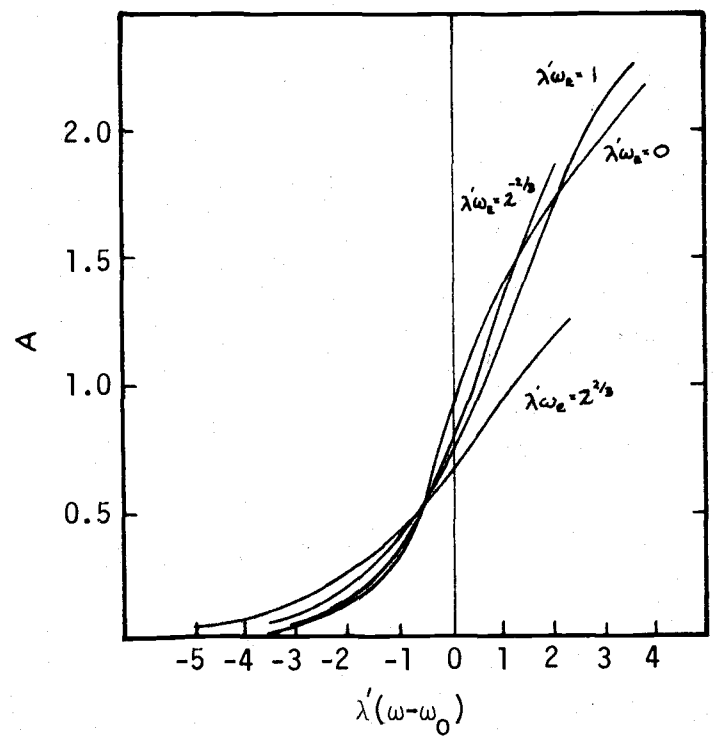

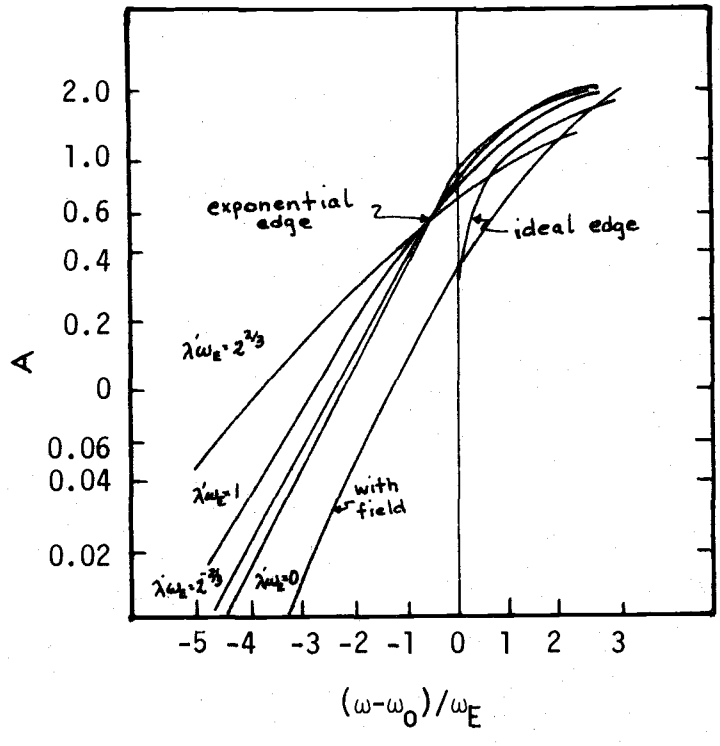

Figure 1. Shift of absorption edge for both ideal and exponential edges.

According to Franz, for $\lambda' (\omega-\omega_o) << 1$, the electric field shifts the absorption edge by an amount,

$$\Delta\omega = - (\lambda'^2 e^2 E^2 / 12\hbar m^*)$$

and the corresponding increase in absorption

$$\Delta\alpha \sim \exp (\lambda'^3 e^2 E^2 / 12\hbar m^*) \qquad (2.3)$$

where λ' is related to the slope of the zero-field absorption curve. This behavior is shown also in Figure 1.

Since the initial calculations of Franz and Keldysh, many workers have contributed to the theory of the effect of the electric field upon the absorption coefficient of solids. In 1963, Tharmalingham (32) obtained the first closed form solution describing electric field effects on the optical absorption at the fundamental edge. Callaway (3) showed that the absorption coefficient should contain fine structure, called "stark steps," due to the periodicity of the lattice. In the weak field limit, the theories of Callaway and Tharmalingham predict identical results. For the ideal band edge the absorption due to the electric field is,

$$\alpha (\omega, E) = \frac{B}{n\omega} m^{*3/2} E^{1/2} \left[\left(\frac{dAi(y_o)}{dy_o}\right)^2_{y_o} - y_o Ai^2 (y_o)\right]$$

and the corresponding $\Delta\alpha$ is,

$$\Delta\alpha = \frac{B}{n\omega} m^{*3/2} \omega_E^{1/2} \left[\left(\frac{dAi(y_o)}{d_y}\right)^2_{y_o} - y_o Ai^2(y_o) - y_o^{1/2} \eta(-y_o)\right] \qquad (2.4)$$

where $y_o = (\omega_o - \omega)/\omega_E$ and B is a constant. The functional form of $\Delta\alpha$ is plotted on an arbitrary scale in Figure 2 as a function of the dimension-less variable y_o which depends upon the energy distance from the gap as well as the magnitude of the electric field to the 2/3 power. The predictions of this theory are listed below:

1. The energy gap should occur very close to the first positive peak,

$$y_o = \frac{\omega_o - \omega}{E} = 0$$

2. The amplitude of the peaks in $\Delta\alpha$ should increase as $E^{1/3}$. The peak heights should never decrease with increasing electric field.

3. For energies below the gap, the asymptotic form of $\Delta\alpha$ becomes (3),

$$\Delta\alpha\ (\omega, E) = \alpha\ (\omega, E) - \alpha(0) = \frac{K\ m^*}{\omega\ (\omega_o - \omega)} \exp\left[-4/3\ \frac{(2m^*)^{1/2}}{\hbar}\ \frac{(\omega_o - \omega)^{3/2}}{eE}\right]$$

where K is a constant.

Using the numbers appropriate to GaAs, Callaway obtained the curves shown in Figure 3.

Review of Previous Experimental Results

The first published experimental attempt appeared approximately two years after Franz and Keldysch's theory. Since then an ever increasing number of articles have appeared in journals. Since most of these are concerned with matching their results with theory and thereby determining physical constants of the materials, experiments are performed at low temperatures. The results of a few selected

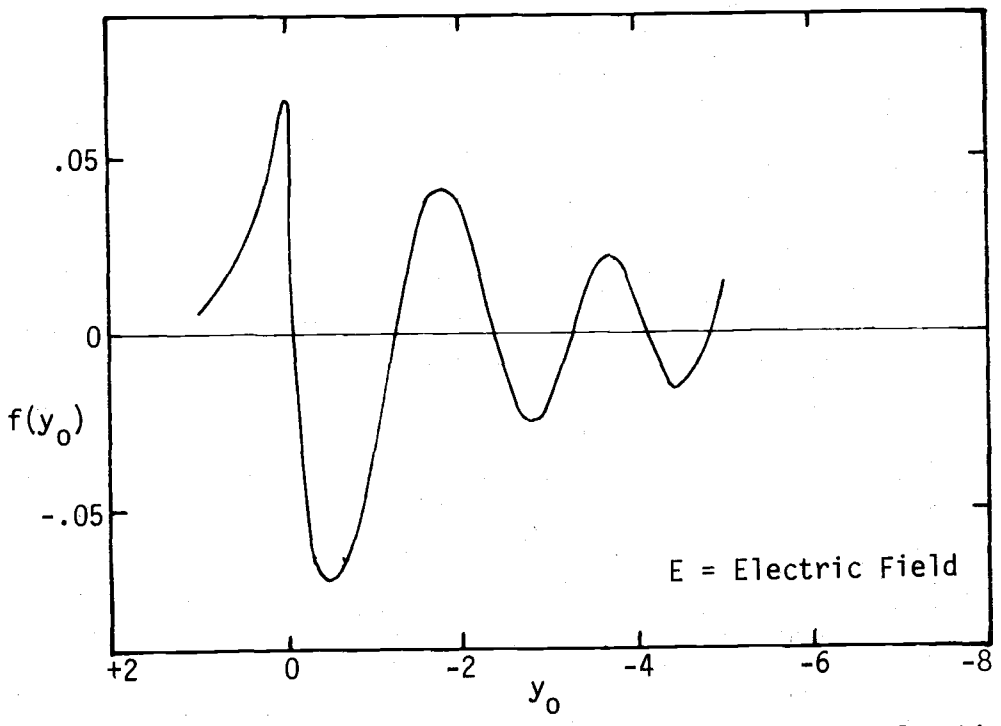

Figure 2. Optional absorption coefficient as a function of energy in the weak field limit.

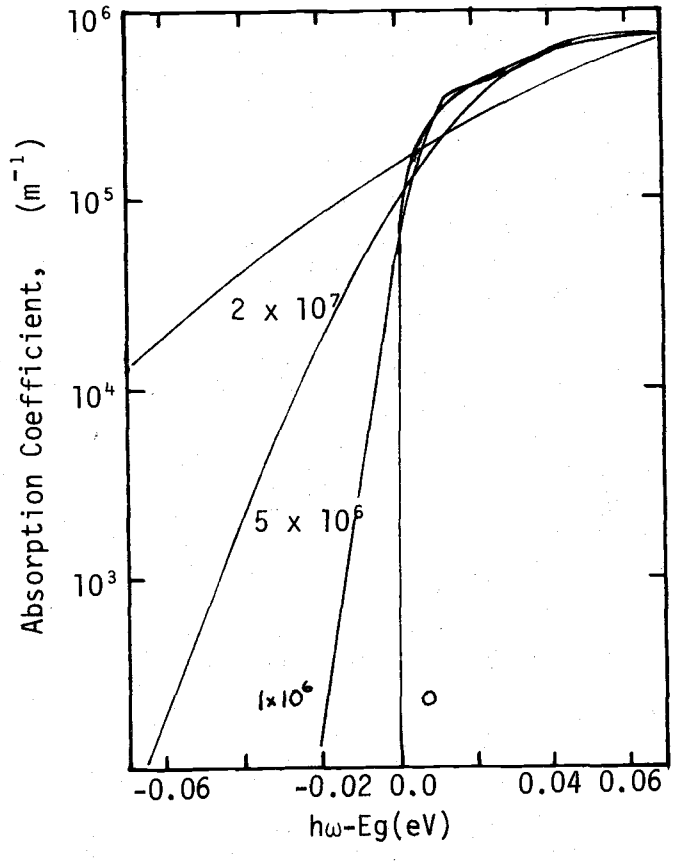

Figure 3. Calculated absorption changes in GaAs using Callaway's model.

articles in which experiments were performed at room temperature are presented. One should note in particular the difficulty in matching experimental results with theory.

In 1960, Williams observed electric field induced light absorption in CdS crystals (35). The high field was produced by utilizing the rectifying contact between CdS and an electrolyte solution. His results are shown in Figures 4 and 5. Note that the shift of approximately 70 Å was obtained for an applied voltage of 120 V and that the shift was directly proportional to the applied voltage. No attempt was made to match this behavior with theory because the field distribution was not known.

The first work which showed the transformation of the direct edge into an exponential edge was reported by Frova and Handler (11) on germanium. By using a reverse-biased p-n junction, they were able to produce almost complete modulation of a monochromatic beam of light. At room temperature, the percentage modulation and fractional change in absorption coefficient are illustrated in Figures 6 and 7.

L. M. Lambert (22) obtained the results shown in Figure 8 for GaAs by placing semi-insulating material between parallel plates, with mylar between the semiconductor and electrodes. The dashed lines are the experimental curves and the solid lines are based on calculations according to Callaway's theory. In order to obtain the experimental curve, any zero-field absorption below the band gap is assumed to be field independent and is subtracted from the field induced absorption. Note that the fit is poor, especially at low fields, and the change in absorption is large at relatively low fields.

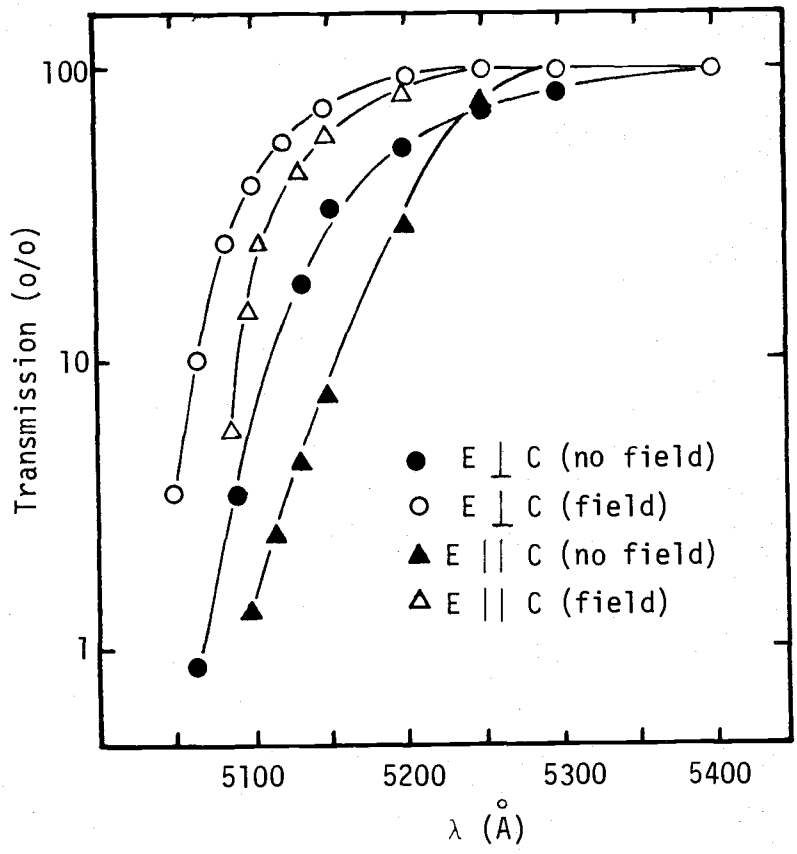

Figure 4. Field induced change in light transmission through CdS crystal.

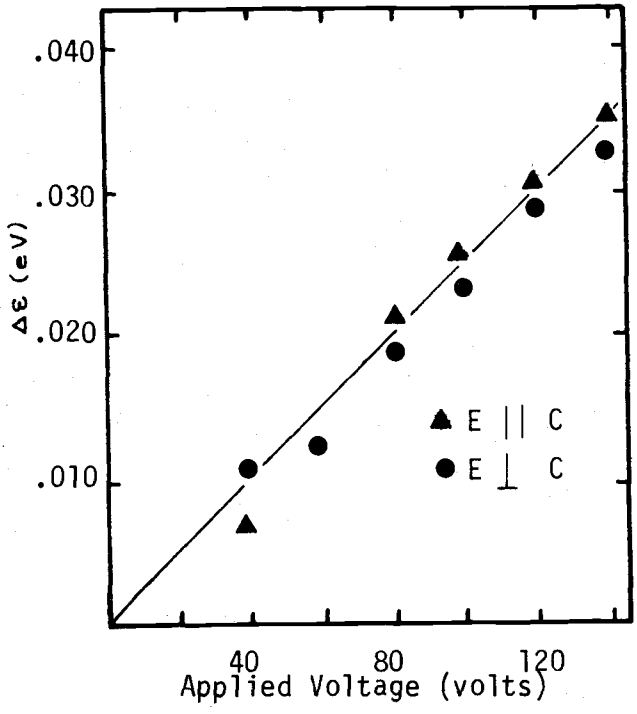

Figure 5. Shift of band edge as a function of applied voltage.

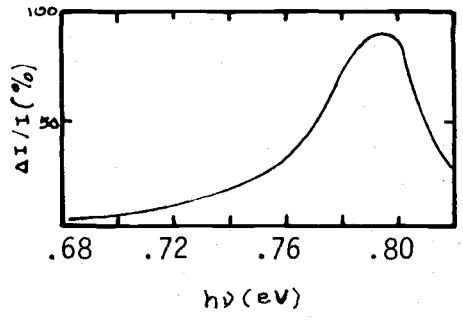

Figure 6. Percent modulation spectrum of Ge p-n junction.

Figure 7. Absorption coefficient spectra of Ge p-n junction.

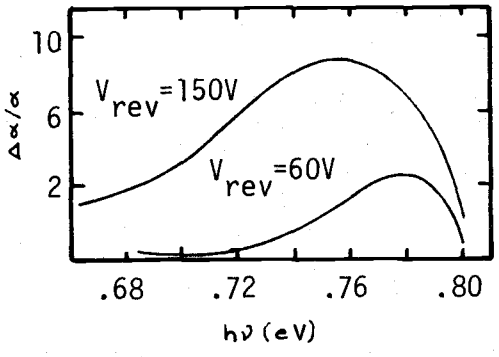

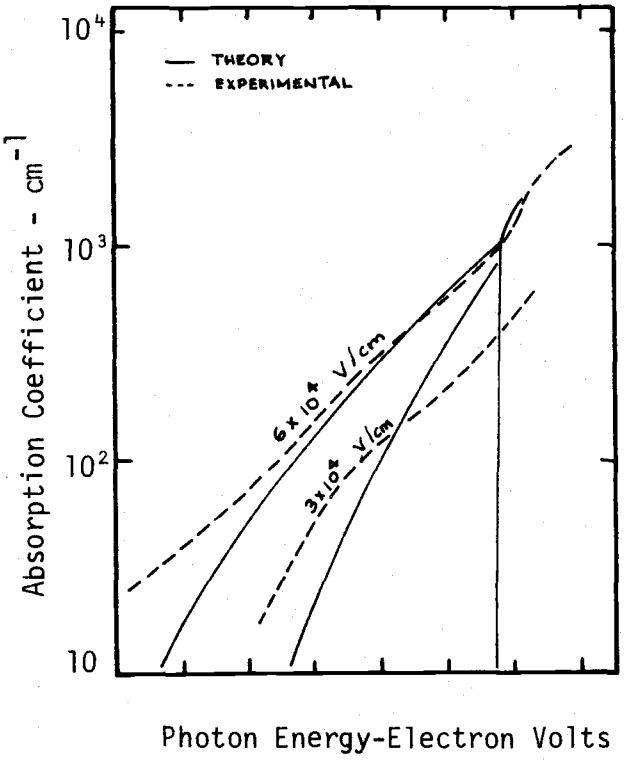

Figure 8. Change in α at 295°K for GaAs.

Perov (28) et al. grew heteroepitaxially 0.2 to 0.5 micron CdS films on mica substrates. Thin semitransparent electrodes were deposited by vacuum evaporation of Cr. The room temperature electro-absorption spectrum of their sample is shown in Figure 9. The figure shows several peaks, but this work is concerned only with the long wave length positive peak. Of interest is the magnitude of this peak. Although the magnitude of $\Delta\alpha$ may seem large, the percentage change in intensity ($\Delta I/I$) is small because the zero-field absorption is large (10^4 cm^{-1}).

Recently at a conference, Honda (19) reported a shift of 120 Å in one micron thick CdS film for an electric field of 8.34×10^4 v/cm. The shift of absorption edges as a function of applied field is shown in Figure 10. At 8.34×10^4 V/cm, he and his co-workers reported a 50 percent modulation of light intensity with wavelength of 5500 Å!

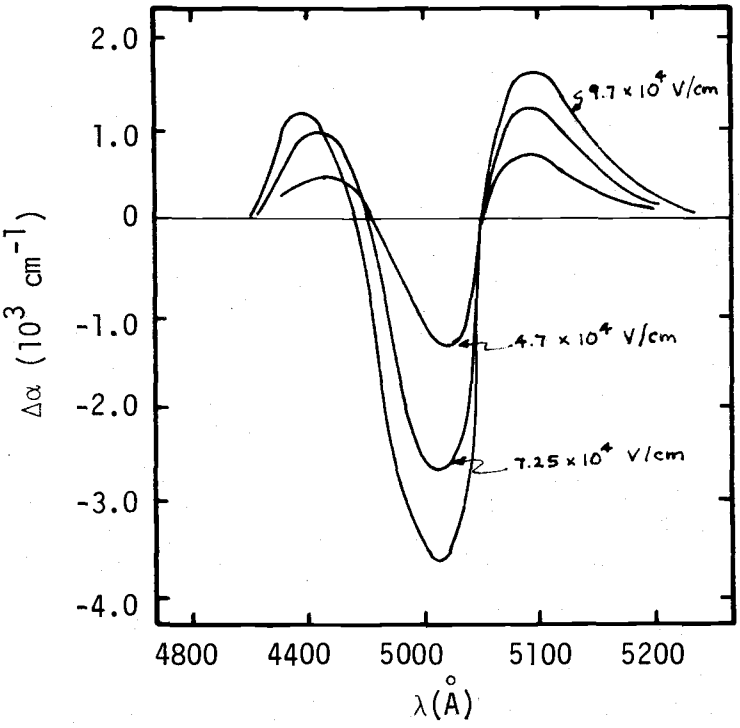

Figure 9. Electro absorption spectrum of CdS film.

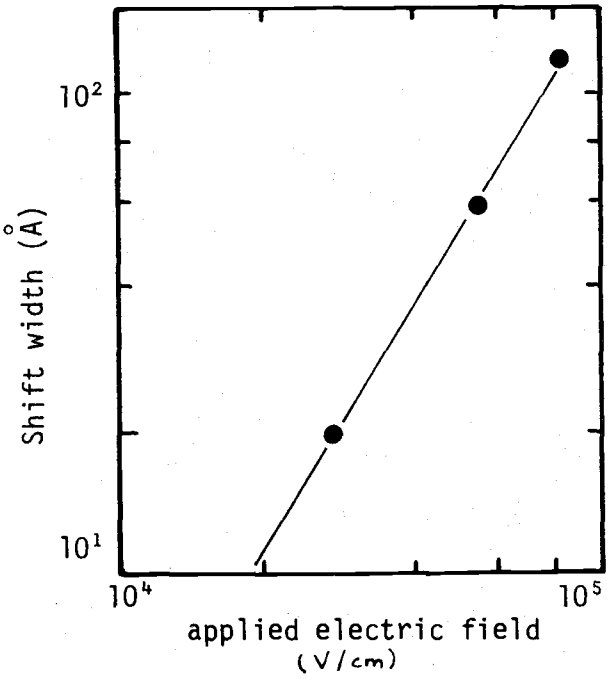

Figure 10. Shift in absorption edge as a function of applied field.

III. DEVICE EQUATIONS FOR LINEARLY VARYING ELECTRIC FIELD

In order to cause an appreciable change in the absorption spectrum of a material, electric fields of the order of 10^5 to 10^6 V/cm and very low current levels are desirable. If the material is an insulator an extremely simple parallel plate capacitor configuration may be used to obtain uniform fields. The electrodes would be of transparent or semitransparent material and the material of interest would act as the dielectric. The advantage of this configuration is that a large region of high electric field can be obtained and analysis is simpler because the theory is based on uniform electric fields. The disadvantage is that a large voltage (of the order of 10^3 volts for 10μm) is necessary to acquire high electric fields.

Since this work involves the use of a semiconductor, the previously mentioned technique cannot be used. Instead, we look to another method in which a space-charge region is created and the field in this region is varied by applying the appropriate bias. Fortunately, space-charge regions exist in several two terminal devices and they are: p-n junction diode, metal-semiconductor diode, and metal-insulator-semiconductor (MIS) diodes. In these devices it is possible to obtain high fields over very short distances and also avoid overheating of the samples which would contribute to electrical breakdown and create uncontrollable additional absorption.

Because the electric field is not uniform, the complex equations for $\Delta\alpha$ and $\Delta I/I$ must be modified so that they would be in terms of the maximum electric field in the space-charge region of the diode. The

method used in arriving at the modified equations were similar to that of Frova and Handler (11).

Electric Field and Depletion Width Expressions for MIS Diodes

The MIS structure is shown in Figure 11 where x_i is the thickness of the insulator and V_a is the applied voltage on the metal field plate. In order to be consistent, let the voltage V be positive when the metal plate is positively biased with respect to the ohmic contact, and V be negative when the field electrode is negatively biased with respect to the ohmic contact.

When the MIS is biased with positive or negative voltages, three possibilities may exist at the semiconductor surface. The diagrams are shown in Figure 12 for n-type semiconductor. Since this work is concerned with obtaining high electric fields in a space-charge region, we are interested in only the depletion mode. In this mode, the small voltage less than zero bends the band upwards and the majority carriers are depleted at the semiconductor oxide surface. The charge distribution, electric field and potential are illustrated in Figure 13. The potential distribution in the space charge region is described by the equation

$$\psi = \psi_s \left(1 - \frac{x}{W}\right)^2$$

where the surface potential is given by

$$\psi_s = \frac{qN_D W^2}{2\varepsilon_s} \quad \text{or} \quad W = \sqrt{\frac{2\varepsilon_s}{qN_D}\psi_s} \tag{3.1}$$

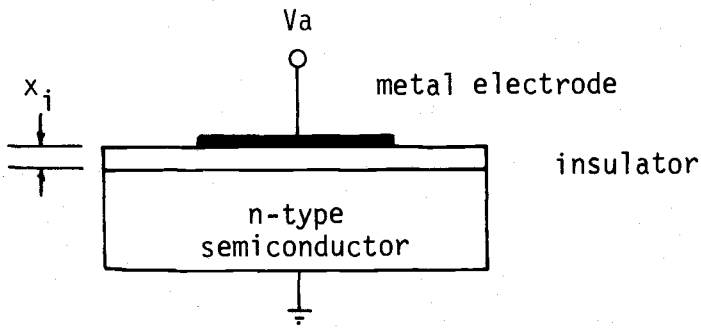

Figure 11. MIS structure.

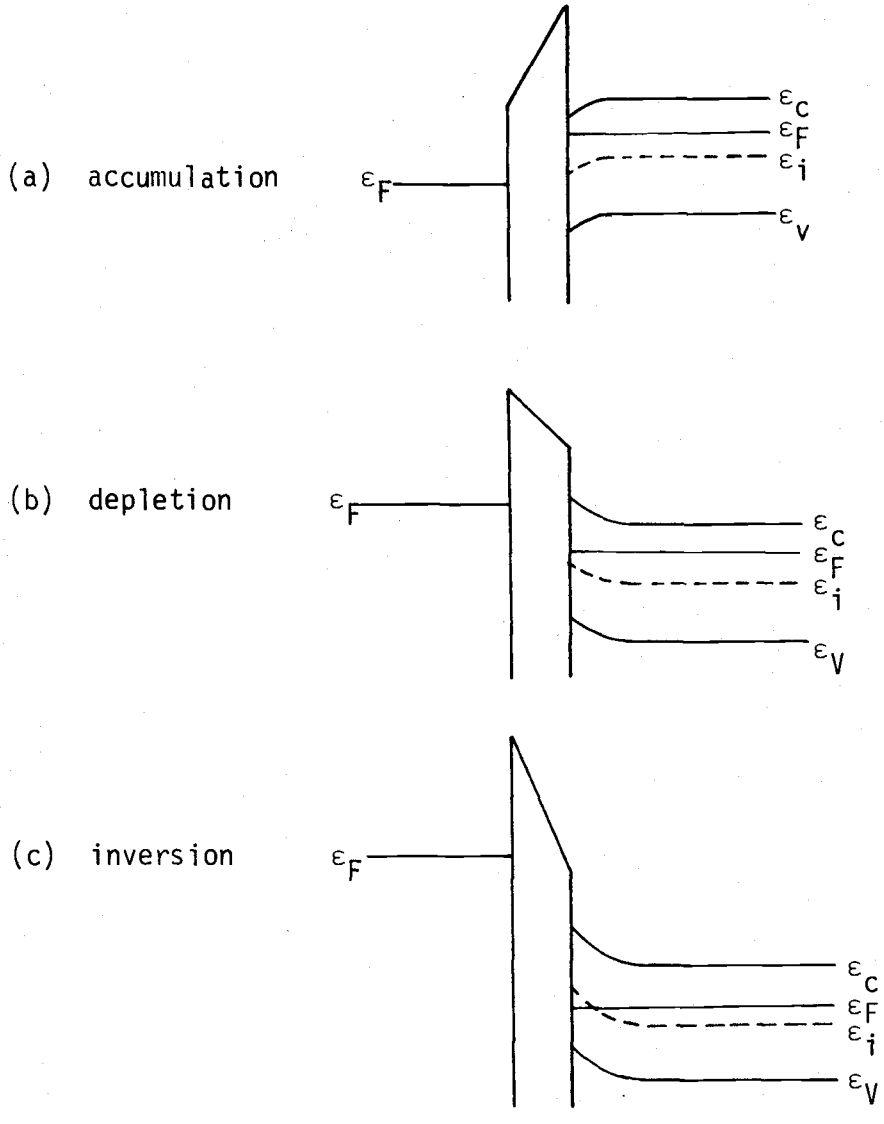

Figure 12. Energy band diagrams for MIS structure with n-type material.

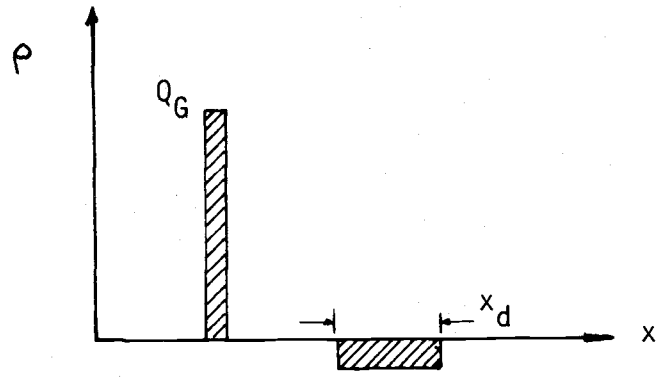

(a) charge distribution

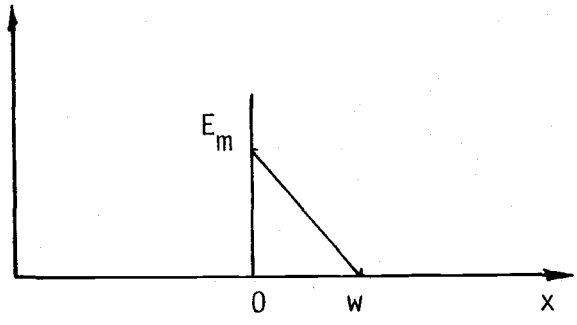

(b) electric field

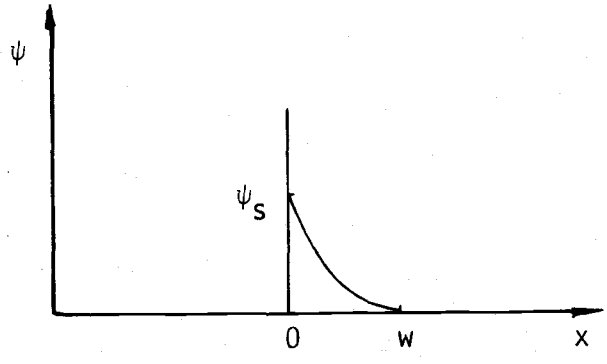

(c) potential distribution

Figure 13

ε_s is dielectric constant of semiconductor

N_D is donor concentration

It follows then that

$$E = -\frac{\partial \psi}{\partial x} = \frac{2\psi_s}{W}\left(1 - \frac{x}{W}\right) = E_m\left(1 - \frac{x}{W}\right) \tag{3.2}$$

or E varies linearly with x as in the case of abrupt junctions.

Electric Field and Depletion Width Variation in Metal-Semiconductor Diodes

In Figure 14 are shown the energy band diagrams for a metal on n-type semiconductor at thermal equilibrium and reverse bias conditions.

If the abrupt approximation is made, i.e., $\rho = qN_D$ for $x < W$ and $\rho = 0$ for $dV/dx = 0$ for $x > W$ where W is the depletion width, the results for the metal-semiconductor barrier are identical to those of the one-sided abrupt p-n junction. The expressions for depletion width, field dependence, and voltage variation are:

$$W = \left[\frac{2\varepsilon_s}{qN_D}\left(V_{bi} - V_a - \frac{kT}{q}\right)\right]^{1/2} \tag{3.3}$$

$$|E(x)| = \frac{qN_D}{\varepsilon_s}(W - x) \tag{3.4}$$

$$V(x) = \frac{qN_D}{\varepsilon_s}(Wx - 1/2x^2) - \phi_{Bn}$$

where V_{bi} is the built-in potential and ϕ_{Bn} is the barrier height of the metal-semiconductor contact.

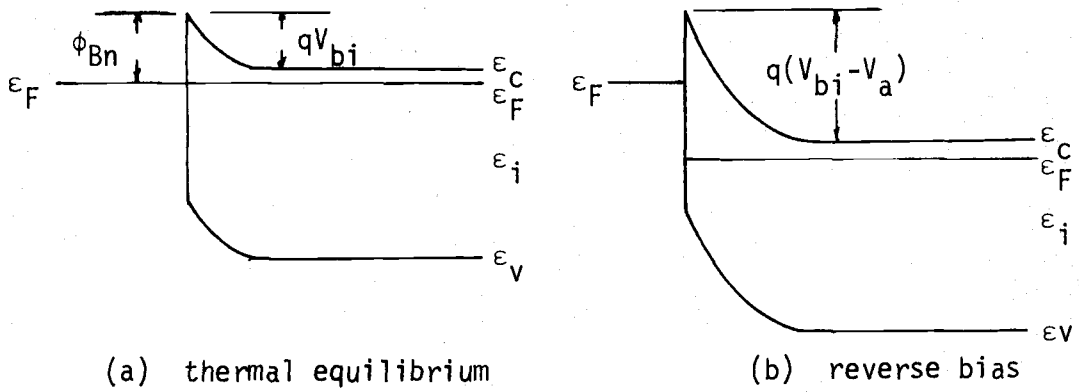

(a) thermal equilibrium (b) reverse bias

Figure 14. Energy band diagrams for Schottky barrier diodes.

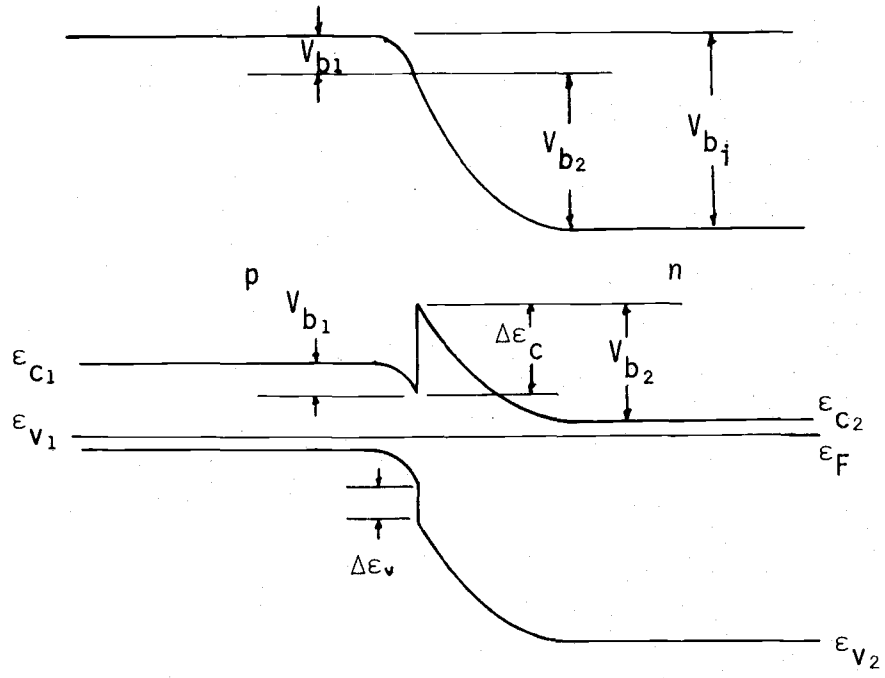

Figure 15. Band diagram of a p-n heterojunction.

Expressions for Electric Field and Depletion Width Variations in p-n Heterojunction Diodes

The present technology does not permit the fabrication of p-n junctions between similar CdS materials, but p-n heterojunctions are possible with CdS as the n-type semiconductor. Figure 15 shows the energy band and potential variation diagram of a p-n heterojunction, a junction formed between a p-type narrow gap semiconductor and an n-type wide-gap semiconductor. Since the Fermi level must coincide on both sides in equilibrium and the vacuum level is everywhere parallel to the band edges and is continuous, the discontinuity in conduction band edges (ΔE_c) and valence band edges (ΔE_v) is invariant with doping in those cases where Eg and χ (electron affinity) are not functions of doping. The total built in potential V_{bi} is equal to the sum of the partial built in voltages ($V_{b1} + V_{b2}$) where V_{b1} and V_{b2} are the electrostatic potentials supported at equilibrium by semiconductors 1 and 2 respectively. V_{bi} is also equal to the difference in work functions of the two materials.

The expressions for depletion width, voltage and electric field variations is obtained by solving Poisson's equation for the step junction on either side of the interface.

The equations for the electric fields and voltages as functions of position are,

$$E_2(x) = \frac{qN_{D_2}}{\varepsilon_2}(x - x_2) \qquad 0 \leq x \leq x_2 \qquad (3.5)$$

$$E_1(x) = \frac{-qN_{A_1}}{\varepsilon_1}(x + x_1) \qquad 0 \geq x \geq -x_1 \qquad (3.6)$$

$$V_2(x) = E_{m2}\left(x - \frac{x^2}{2x_2}\right) + (V_{b1} - V_{a1}) \qquad 0 \leq x \leq x_2 \qquad (3.7)$$

$$V_1(x) = E_{m1}\left(x + \frac{x^2}{2x_1}\right) + (V_{b1} - V_{a1}) \qquad 0 \geq x \geq -x_1 \qquad (3.8)$$

Where

$$V_a = V_{a1} + V_{a2}$$

$$E_{m1} = \frac{-qN_{A1}x_1}{\varepsilon_1}\,, \quad E_{m2} = \frac{qN_{D2}x_2}{\varepsilon_2}$$

and

$$\frac{E_{m1}x_1}{2} = -(V_{b1} - V_{a1}), \quad \frac{E_{m2}x_2}{2} = V_{b2} - V_{a2}$$

The relative voltages supported in each of the semiconductors are,

$$\frac{V_{b1} - V_{a1}}{V_{b2} - V_{a2}} = \frac{N_{D2}\varepsilon_2}{N_{A1}\varepsilon_1}\,.$$

Most of the potential difference occurs in the more lightly doped region for nearly equal dielectric constants.

By manipulation of the above equations one then obtains the expression for depletion widths,

$$x_1 = \frac{A}{N_{A1}}(V_{bi} - V_a)^{1/2}$$

$$x_2 = \frac{A}{N_{D2}}(V_{bi} - V_a)^{1/2}$$

where

$$A = \left[\frac{2\varepsilon_1 N_{A1} \varepsilon_2 N_{D2}}{q\,(\varepsilon_1 N_{A1} + \varepsilon_2 N_{D2})} \right]^{1/2}$$

Development of $\Delta I/I$ in Terms of the Maximum Electric Field in the Device

In each of the methods of applying an electric field to a semiconductor, the electric field varies linearly with distance in the space charge region. Let us now consider the effect of a step increase in voltage on the light intensity transmitted through the junction.

According to Frova and Handler (11), the difference of the transmitted light due to increasing the width of the space charge region as well as the maximum value of E will be

$$\ell n \left(\frac{I'}{I_o}\right) - \ell n \left(\frac{I}{I_o}\right) = \int_o^b \alpha'(x)dx - \int_o^b \alpha(x)dx$$

where I_o is the intensity of the incident light, I' and I are the intensities of the emergent light, and $\alpha'(x)$ and $\alpha(x)$ are the absorption coefficients of the two states of reverse bias. From Figure 16, it may be seen that the region between $W + \Delta W$ and b is unaffected by the bias change and may be neglected.

The equation may be re-written as the sum of four integrals,

$$\ell n \left(\frac{I'}{I}\right) = - \int_{\Delta W}^{W+\Delta W} \alpha'(x)dx + \int_o^{\Delta W} \alpha'(x)dx - \int_o^{W} \alpha(x)dx - \int_W^{W+\Delta W} \alpha(x)dx$$

The first integration is over the crosshatched region II of Figure 16 while the third integral is over the crosshatched region I of the same

figure. Since α is only a function of magnitude of the electric field, the first and third integrals cancel each other. Hence,

$$\ell n \left(\frac{I'}{I}\right) = -\left[\int_0^{\Delta W} \alpha'(x)dx - \int_W^{W+\Delta W} \alpha(x)dx\right]$$

The value of α in the region near W where the electric field is zero may be written as $\alpha(0)$ and is equal to the intrinsic absorption coefficient of the crystal. I' may be expressed as $I + \Delta I$ and substituted into the previous equation in order to obtain an expression for $\Delta I/I$ which is the quantity of interest in our experiments.

$$\ell n \left(\frac{I'}{I}\right) = \ell n \left(\frac{I+\Delta I}{I}\right) = -\int_0^{\Delta W} \alpha'(x)dx - \alpha(0)\ \Delta W$$

or

$$\frac{\Delta I}{I} = \exp\left[-\left[\int_0^{\Delta W} \alpha'(x)dx + \alpha(0)\,\Delta W\right]\right] - 1 \qquad (3.9)$$

The evaluation of $\Delta I/I$ is made rather difficult due to the integral in the exponential. The absorption coefficient $\alpha'(x)$ is a function of the electric field which is in turn varying with position within the space-charge region (see Figure 17).

For a linear field variation we know that,

$$E = E_m \left(1 - \frac{x}{W}\right)$$

and

$$dE = \frac{-E_m}{W} dx = -A dx$$

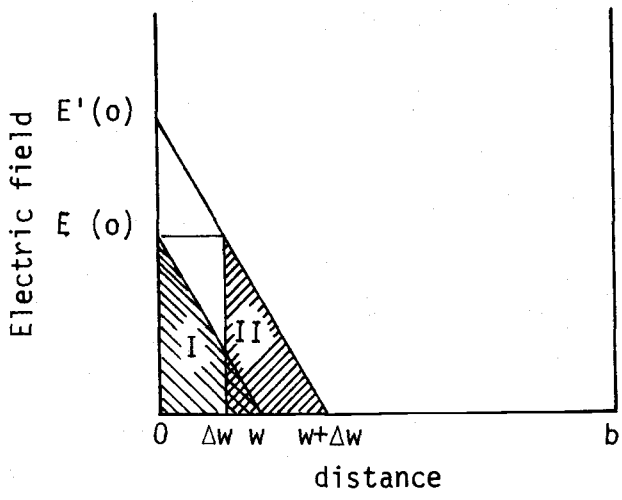

Figure 16. Electric field in space charge region for two values of applied voltage.

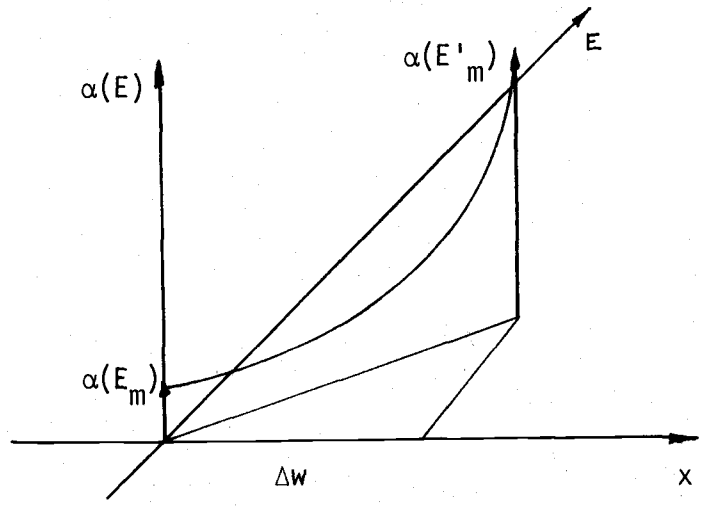

Figure 17. Three-dimensional plot of E, x, and α.

Now we re-write the integral

$$\int_0^{\Delta W} \alpha'(x)dx = \int_{E_m}^{E'_m} \frac{\alpha'(E)dE}{A} .$$

According to Franz,

$$\alpha'(E) = \alpha_o \exp(\lambda'^3\omega_E^3) = \alpha_o \exp(\lambda'^3 e^2E^2/12\hbar m^*)$$

$$= \alpha_o \exp(F^2E^2)$$

where

$$F^2 = \frac{\lambda'^3 e^2}{12\hbar m^*}$$

Then

$$\frac{1}{A}\int_{E_m}^{E'_m} \alpha'(E)dE = \frac{1}{A}\int_{E_m}^{E'_m} \alpha_o e^{F^2E^2} dE .$$

By letting $K = F^2E$ the integral becomes

$$\frac{1}{A}\int_{E_m}^{E'_m} \alpha_o e^{F^2E^2} dE = \frac{1}{A}\int_{E_m}^{E'_m} \alpha_o e^{KE} dE$$

Now we stop and try to find out how K varies with electric field. In Figure 18 the zero-field absorption curve is shown according to Dutton. The absorption curves in the presence of the applied field are according to the theory of Franz. In Figure 19 is

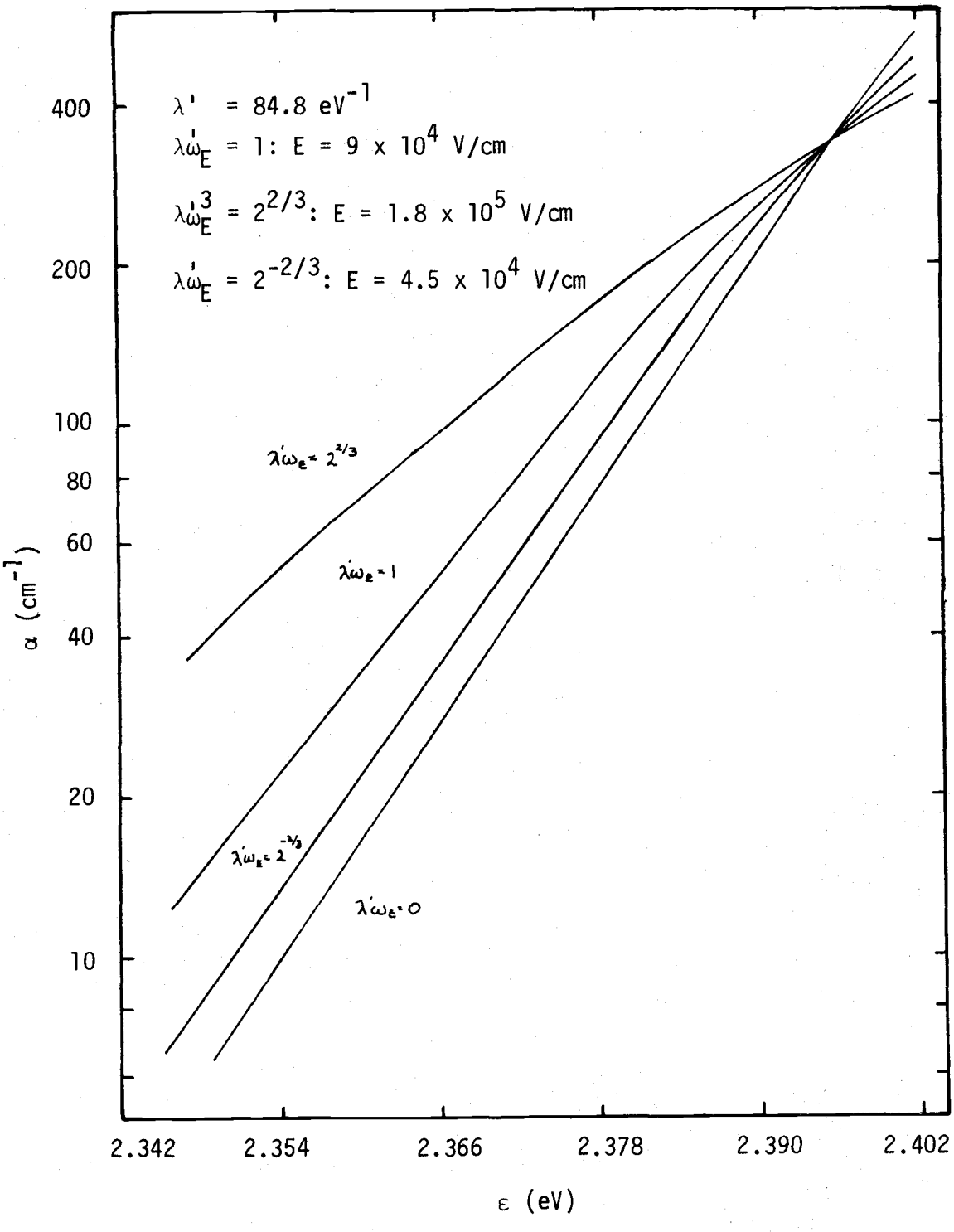

Figure 18. Calculated change in absorption coefficient as a function of applied field in CdS.

shown the corresponding $\Delta\alpha$ curves for uniform electric fields. By plotting α as a function of electric field we see that for a constant wave length K is a slowly varying function of electric field and could be regarded as a constant (see Figure 20). Hence,

$$\frac{1}{A}\int_{E_m}^{E_m'} \alpha_o e^{KE} dE = \frac{\alpha_o}{Ak}\left(e^{KE_m'} - e^{KE_m}\right)$$

$$= \frac{\alpha_o}{AK} e^{KE_m}\left(e^{K(E_m'-E_m)} - 1\right) .$$

The expression for $\Delta I/I$ is now written as,

$$\frac{\Delta I}{I} = \exp\left(-\frac{\alpha_o}{AK} e^{KE_m'} + \frac{\alpha_o}{AK} e^{KE_m} + \alpha_o \Delta W\right) - 1$$

$$= \exp - \{(c\alpha'(E_m) - c\alpha'(E_m) + \alpha_o)\Delta W\} - 1 \quad (3.10)$$

where $c = 1/KE_m$ and $c' = 1/KE_m'$.

For diodes E_m is due to the built-in voltage and is of the order of 10^4 V/cm. The term KE_m then is $<< 1$ and we can say that

$$\frac{\Delta I}{I} = \exp\left(-\frac{\alpha_o}{AK} e^{KE_m'} + \frac{\alpha_o}{AK} + \alpha_o \Delta W\right) - 1$$

or

$$\frac{\Delta I}{I} = \exp\left[-(\Delta\alpha_{eff}\Delta W)\right] - 1 \quad (3.11)$$

where $\Delta\alpha_{eff} = [c\alpha(E_m') - (c + 1)\alpha_o]$.

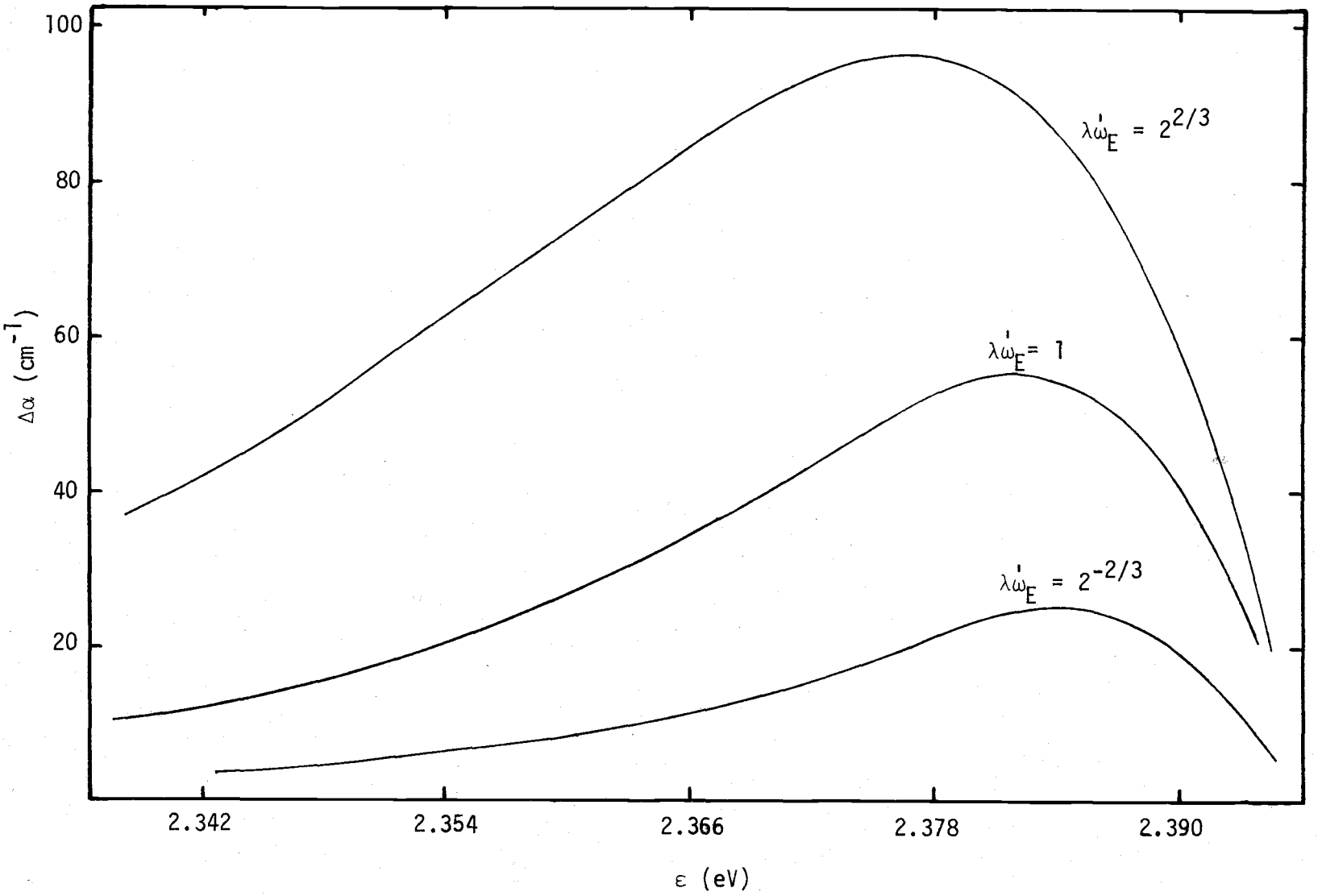

Figure 19. Absorption coefficient change spectra for uniform electric field.

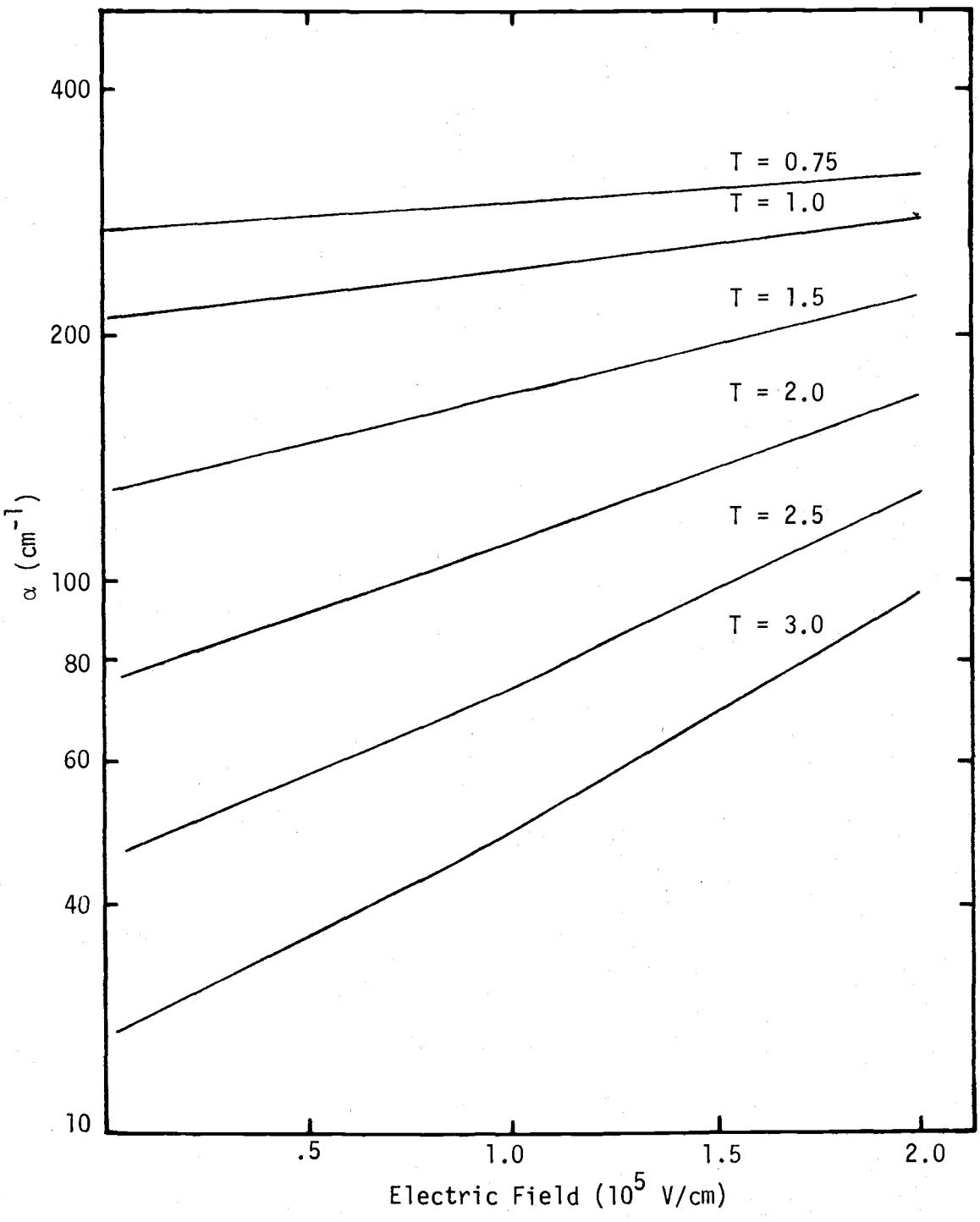

Figure 20. Variation of absorption coefficient with applied electric field with λ' $(\omega-\omega_o)$ as parameter.

This expression is similar to the one obtained in the uniform field case of W. Franz (9). It is evident that once $\Delta\alpha_{eff}$ is known, curves for $\Delta I/I$ can also be drawn. For small values of $\Delta\alpha_{eff}\Delta W$, one could use the first two terms of the series expansion of the exponential and arrive at an expression similar to that in (11), i.e.,

$$\frac{\Delta I}{I} = - \Delta\alpha_{eff} \Delta W \ . \qquad (3.12)$$

Figure 21 shows the behavior of $\Delta\alpha_{eff}$ for several values of maximum electric fields. These curves have to be generated for the material of interest before computing the expected magnitudes of $\Delta I/I$.

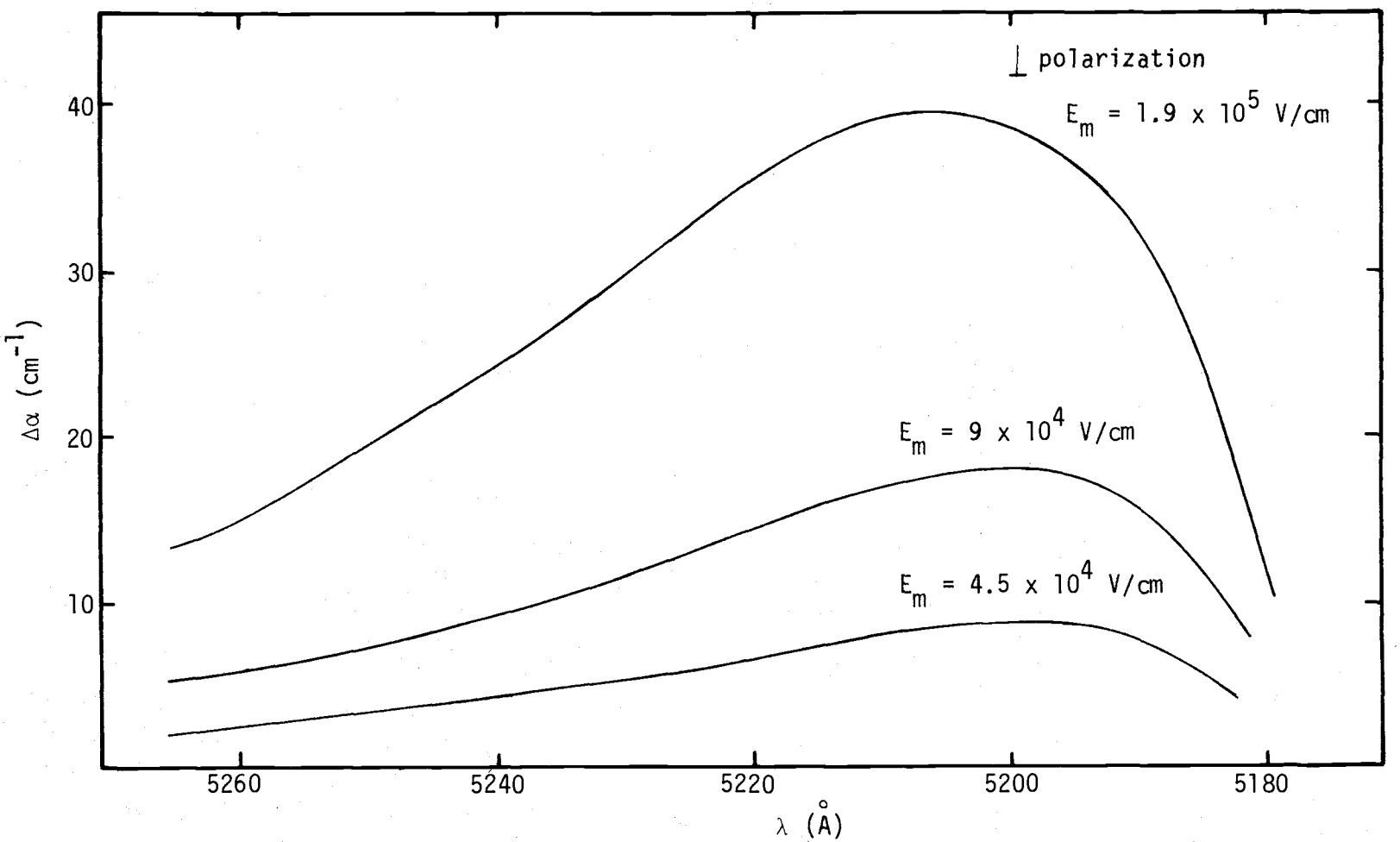

Figure 21. Absorption coefficient change spectra for linear electric field.

IV. DESIGN CONSIDERATIONS

In the previous chapters we have discussed the theory which explains the operation of our proposed devices. Now we will deal with the practical aspects which are of prime importance in the "real world."

Being in a position of limited resources and financial support we have the following general requirements imposed on our design considerations:

(1) The energy gap of the material should be such as to place its band edge in the visible region. The most important reason for this is that our monochromator is most efficient in the visible region and one of our photomultiplier tubes has a strong response in the visible region. Another reason is that if the effect is large enough to be practical, interest would most probably be in the visible light range.

(2) The material should be readily available and fabrication procedures are simple enough to be performed in our solid state electronics laboratory.

With these in mind we now proceed to discuss the factors involved in arriving at the choice of material, device geometries and fabrication processes.

Material Selection

According to Keldysh (21), the shift in absorption edge for a fundamental edge is given by the expression,

$$\Delta\omega = \frac{1}{\hbar}\left[(eE)^2 \frac{\hbar^2}{m^*}\right]^{1/3} \qquad (4.1)$$

It is clear, as far as the material property is concerned, that the magnitude of the edge shift is inversely proportional to the cube root of the reduced effective mass m^*. Therefore, it is desirable that the material possess small effective mass.

For a material with a direct allowed edge but whose absorption coefficient is already exponential below the gap, the expression for the edge shift is,

$$\Delta\omega = -(\lambda'^2(eE)^2/12\hbar m^*) \ . \qquad (4.2)$$

Now the shift is not only inversely proportional to the reduced effective mass but also proportional to the square of the slope λ' of the experimental zero field absorption curve. Hence a steep zero field slope is desirable which will require that the crystal be pure and unstained, as well as undamaged by processes such as lapping.

We used single crystal CdS in this project because we were able to acquire this material. The properties of this material fulfills most of the requirements. The energy gap is direct and at a value of 2.40eV (6) which is in the visible region. The reduced effective masses are equal to (34),

$$m^*_{\perp} = .316\ m_o \text{ and } m^*_{||} = .393\ m_o.$$

The slope s of the absorption curve is given by Dutton (6) as 2.17 or $\lambda' = s/kT = 84.8eV^{-1}$ at room temperature.

Semitransparent Electrodes

It is evident in the discussion of field induced absorption in space charge regions of diodes that any electrode used to apply the field should be transparent to the incident light at the wave lengths of interest. We are able only to approximate this condition with a very thin metal film. Au was chosen as electrode material mainly because of its resistance to oxidation which changes the electrode properties considerably for very thin films.

Device Geometry

Maximum reverse breakdown voltages are desirable in order that large changes in transmitted light are produced. Corresponding with the reverse breakdown voltage are maximum electric fields. It is obvious that circular diode patterns should reduce the edge breakdown effects which are pronounced in any patterns having sharp corners. We also know that the critical field of the material increases slightly with an increase with semiconductor doping which makes moderately doped material better suited for high electric fields.

The area of the active region is made large enough in diameter to extend over the slit width of the monochromator, and to insure maximum change in transmitted light intensity. The dead region, i.e., region outside the junction should be minimized (within practical limits) in order to minimize unwanted absorption and again insure maximum change in transmitted light intensity.

Choice of Fabrication Processes

For the sake of saving a great deal of time, many processes developed in the solid state laboratory of this department are used in the fabrication of devices. The polishing of the crystal, however, was done manually to obtain mirror-like finishes. Other methods of polishing the surface were tried but without success.

V. DEVICE FABRICATION AND EVALUATION PROCEDURES

Some of the processes used in the fabrication of the devices were standard procedures used in the fabrication of silicon integrated circuits in the solid state laboratory. Other processes, however, had to be obtained from the literatures; for example, the formation of a p-type region on CdS. Still other techniques had to be devised for proper handling of the crystal after its surface was polished.

The device evaluation techniques were standard techniques and can be found in literature or text books.

Fabrication Procedures for Various Diode Configurations

Only the general processes will be outlined in this section. The details of each process can be found in Appendix I. The first few steps involve the preparation of the crystal and the procedure is the same for all configurations.

(a) The crystals are cut into 10-20 mil. thick wafers with the diamond saw. Rectangular samples approximately 0.5 cm x 0.5 cm are then cut from the wafers.

(b) The large areas of the crystals are lapped and polished mechanically.

As shown in Figure 22 (a, b, c) steps are different from each configuration and will be mentioned separately.

(1) MIS Diode

(c) The sample is etched for a short while ($\sim$ 30 seconds) in 10:1 HCl.

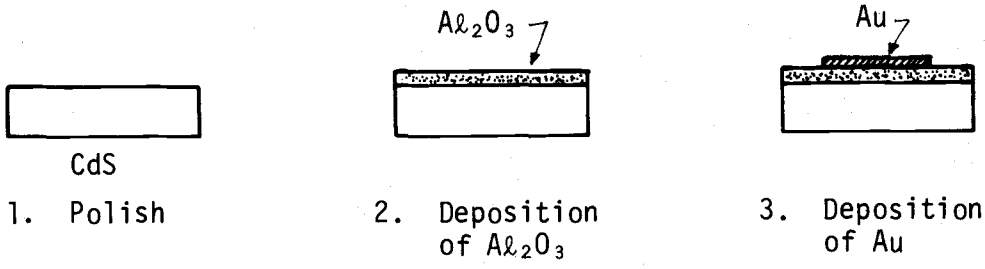

(a) MIS

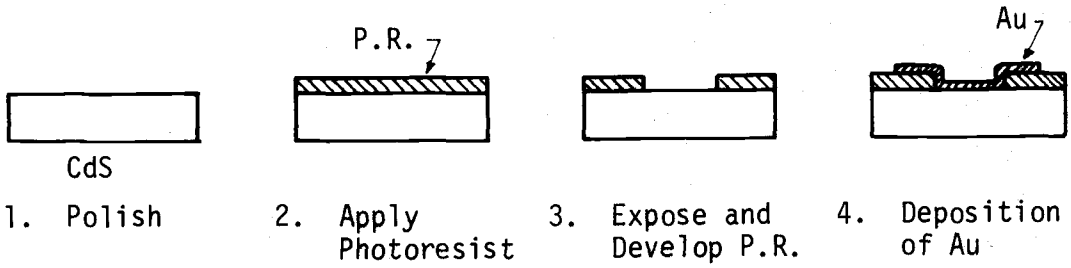

(b) Metal-Semiconductor

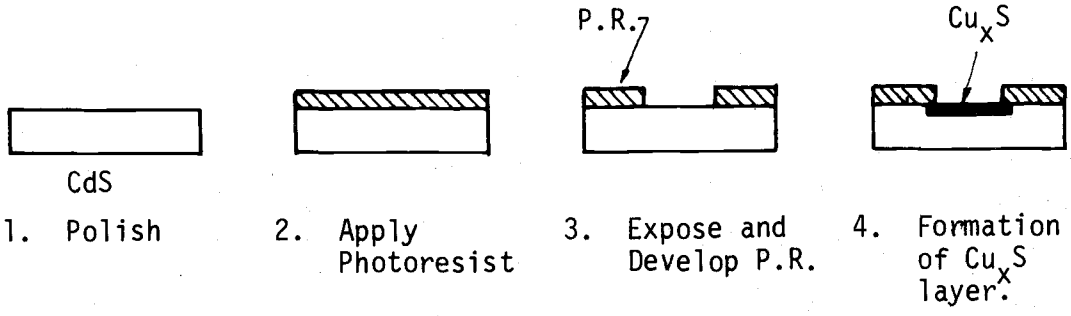

(c) P^+-N heterojunction

Figure 22. Fabrication steps for different configurations

(d) 2000-4000 Å of Al_2O_3 is deposited on one surface of the crystal by the evaporation of sapphire with an electron beam gun.

(e) The sample is removed from the high vacuum system and placed in a diffusion pump system, in which a semitransparent layer of Au is deposited on the oxide through a metal mask. The area of the electrode is .01 and .001 $in.^2$ for the samples. The sheet resistivity of the Au film is 500 Ω/□.

(f) The sample is placed on an Indium foil on the holder. A spring clip presses the device firmly against the foil, thereby assuring an ohmic contact to the rear face.

(g) Contact to the top electrode is made by attaching to it .002 in. gold wire with silver print.

The sample is ready to be tested.

(2) Metal-Semiconductor Barrier

(c) Photo-resist is applied to one surface of the crystal.

The photo-resist is used to define the active area of the device.

(d) Standard procedures are used to expose and develop the photo-resist. An active area .075 in. in diameter is defined.

(e) The exposed surface is etched lightly with dilute solution of HCl for 30 sec.

(f) The sample is then mounted on the holder.

Pressure ohmic contact to rear of crystal.

(g) An aluminum foil mask is placed over the front surface and placed in the diffusion pump system.

(h) A semitransparent film of Au (100-2 K Ω/□) is deposited on the front surface of the crystal through the foil mask.

(i) Contact to the Au film is made in the same manner described previously.

(3) P-N Heterojunction

(c) Same as part IV-2c.

(d) Same as part IV-2d.

(e) Same as part IV-2e.

(f) The sample is dipped in a solution of CuCl at 80°C for five minutes. According to Gill (2) a 0.5 micron layer of Cu_xS should have formed on the exposed CdS.

(g) The crystal is then heated in air for one minute at 250°C.

(h) The sample is mounted on the holder with the CdS pressed against the Indium foil.

(i) .002 in. Au wire is connected to the Cu_xS region by means of silver print.

Description of Measurement Techniques

(1) I-V Characteristics

The current-voltage characteristics were measured with the Tektronix 576 curve tracer. Of interest is the current level at various reverse bias voltages. Before each applied voltage optical measurement the current through the sample and voltage across the sample is measured with a Tektronix 514 dual-trace oscilloscope.

(2) Optical Transmission Spectra

In order to obtain the optical transmission spectra of the samples and measure the change of their transmitted light intensities as function of applied voltages, the equipment connected as shown in the block diagram of Figure 23 was used.

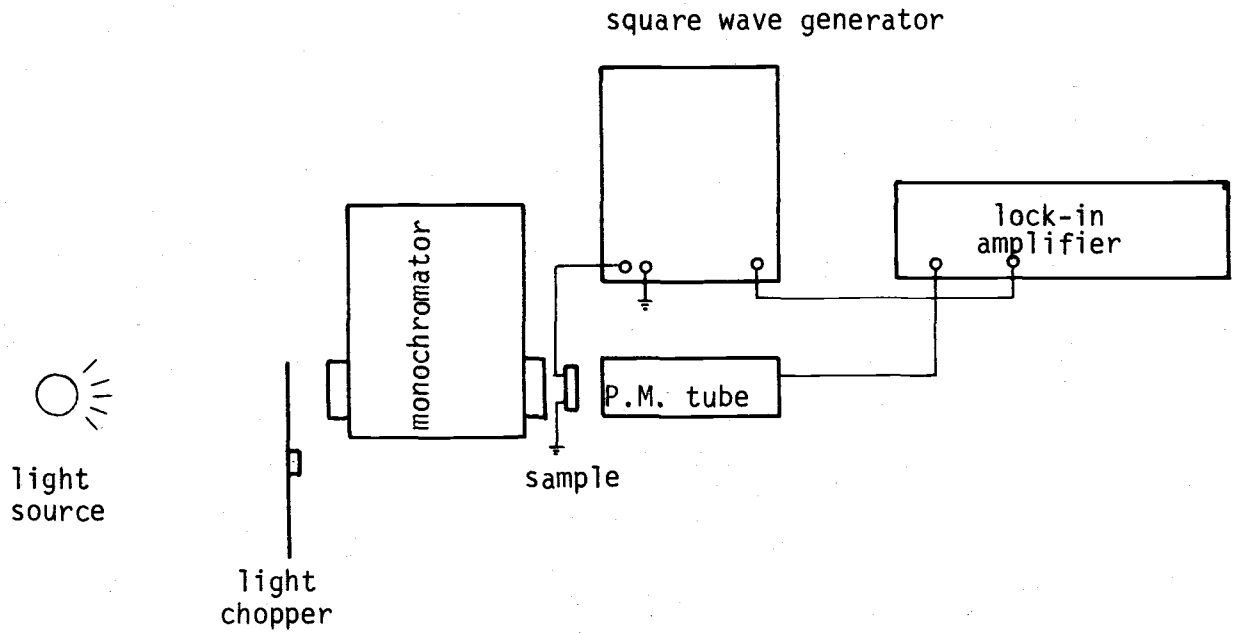

Figure 23. Block diagram of experimental apparatus used to measure transmission spectra.

The light source is a Bausch and Lomb tungsten lamp. The light is chopped with a mechanical chopper at 14 Hz. Selection of wave length is done by means of the Jarrell-Ash 82-410 monochromator whose resolution is 6 Å for a slit width of 100 microns. The transmitted light in the visible region is detected with an RCA 931A photomultiplier tube with an S-4 response. The output of the photomultiplier is measured by the Princeton Applied Research Lock-in Amplifier/Phase Detector model 121 which is capable of measuring one part in 10^5.

The zero-field transmitted light intensity I is determined by the Lock-in amplifier reading with the sample in and light source being chopped at 14 Hz. I' would then be the lock-in amplifier reading with a reverse-bias applied to the sample and ΔI is I-I'. By taking the quotient of (I-I')/I we obtain $\Delta I/I$. However, since our "home made" mechanical light chopper was noisy, we decided not to use this method of measuring ΔI. Instead, we had to use a d-c light source and chop the bias voltage to the sample. ΔI is now proportional to the magnitude of the lock-in amplifier reading. The chopping frequency of the bias voltage is between 40 to 400 Hz. The ratio $\Delta I/I$ should be the same, provided the waveforms of ΔI and I are the same, which is the case here.

The disadvantage of the latter method is that it does not differentiate between positive and negative changes in ΔI. Since we are interested only with changes in the transmitted light intensities occurring below the band edge, the latter method is just as good. At room temperature, ΔI is only negative below the band edge.

In order to obtain the zero-field transmission spectra of the samples, the sample-out readings of the lock-in amplifier are recorded.

The ratio of I to I_o is then formed where I_o is the sample-out reading. For wave lengths above 5340 Å, the quotient is constant. We will assume that there is very little absorption and whatever is not transmitted is reflected. Hence, we will use this value as 100 percent transmission.

The light is polarized by a polarizer placed in front of the monochromator. A Corning CS 1-69 filter was placed at the input to the monochromator to allow only the desired wave lengths to enter the monochromator.

VI. RESULTS AND DISCUSSION

In this chapter the device characteristics are presented and comments are made on the curves when it is thought to be necessary. We also attempt to see whether there would be a close agreement between our experimental results and our calculations based on the theory of Franz.

Presentation of Characteristics of Various Diodes

(1) MIS Diodes

Figure 24 shows the unpolarized transmitted intensity spectra for MIS diodes no. 1 and no. 2. The parallel and perpendicular polarization curves, of MIS 2, shown also in Figure 24, are separated by approximately 40 Å which is in agreement with Dutton (6).

The percentage changes in transmitted light intensity caused by MIS 1 and MIS 2 for an applied voltage of 4 volts are shown in Figure 25; the incident light being unpolarized. The magnitudes are comparable for both diodes and are the smallest observed of all configurations. Approximately 500 μA flowed through MIS 1 and 80 μA flowed through MIS 2 during the reverse-bias cycle. The current densities, however, are nearly the same and insufficient to alter the sample temperature significantly (see Appendix III).

With unpolarized light of λ = 5190 Å incident upon MIS 2, the quantity $\Delta I/I$ changes linearly with applied voltage as in Figure 26. For a linear electric field variation in the space-charge region of

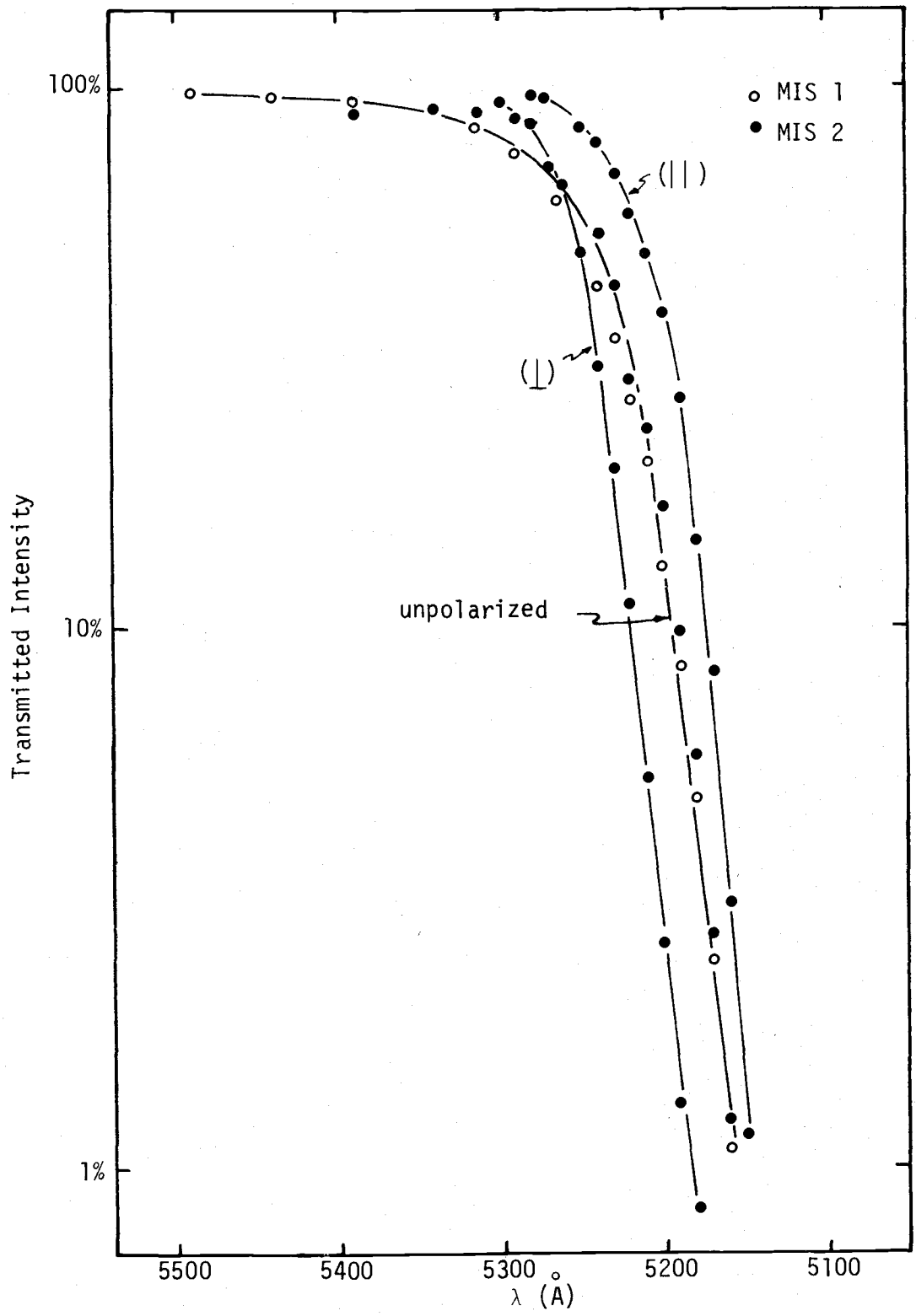

Figure 24. Transmitted intensity spectra for MIS 1 and MIS 2.

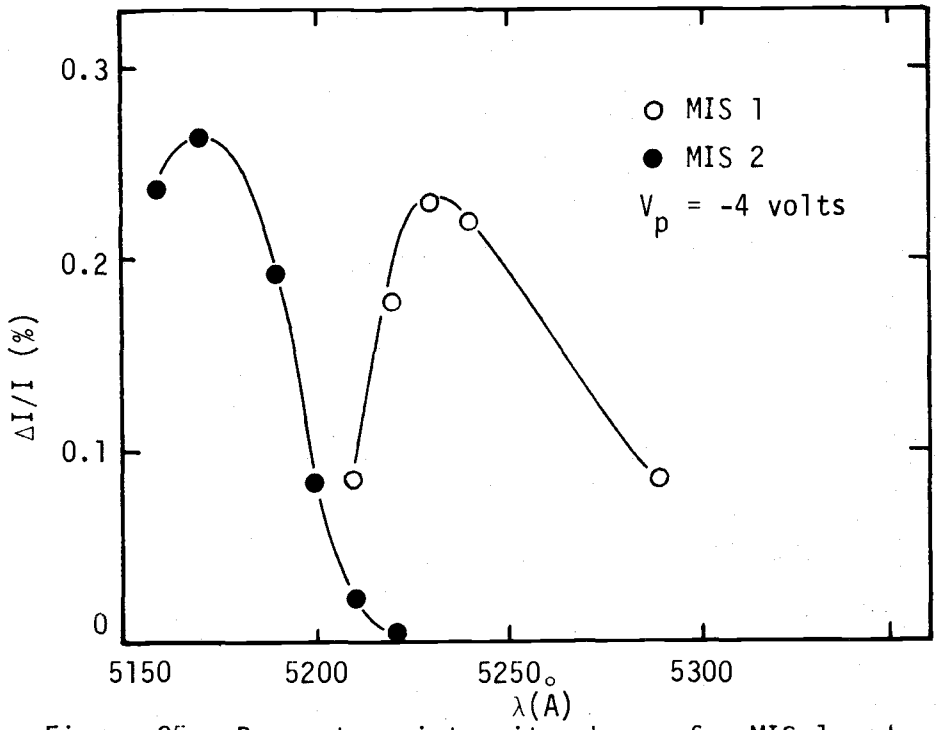

Figure 25. Percentage intensity change for MIS 1 and MIS 2 with unpolarized incident light.

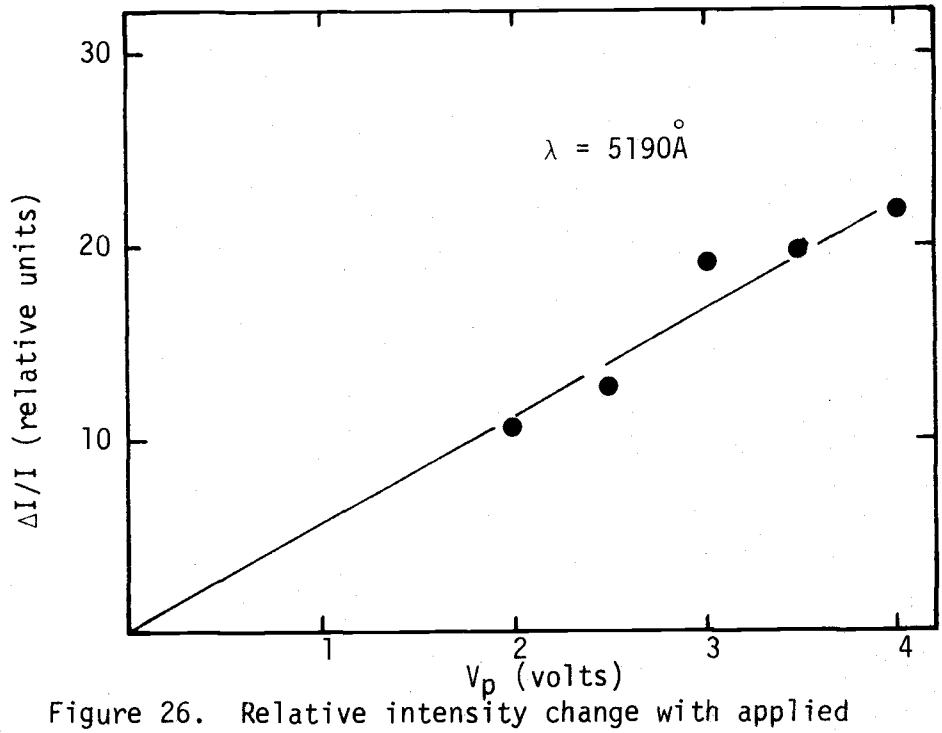

Figure 26. Relative intensity change with applied voltage on MIS 2.

the semiconductor, a linear dependence of $\Delta I/I$ on voltage implies that $\Delta I/I$ is proportional to the square of the maximum electric field, i.e.,

$$\Delta I/I = CE_m^2$$

where C is a proportionality constant.

Figure 27 shows the percentage change in transmitted light intensity for different light polarizations incident upon MIS 2. The applied voltage is again 4 volts. The parallel polarization spectrum is broad and flat while the perpendicular polarization spectrum has a maximum at λ = 5220 Å.

If we define the bandwidth as being the region between the full-width half-maximum points we can compare the bandwidths of the devices. The bandwidths for MIS 1 and MIS 2 are 50 Å with unpolarized incident light. The bandwidth decreases to 40 Å when perpendicularly polarized light is incident on MIS 2. This bandwidth is of interest if the device is to be used as a variable intensity filter.

The advantage of this configuration is that it eliminates the problem of edge breakdown, which is a limiting factor as we shall see later. However premature breakdown, due to pinholes in the insulators, is still observed in our samples. Large area pinhole-free films are difficult to obtain. Another disadvantage, is that in this configuration some of the voltage appears across the insulator, which is undesirable. The maximum surface potential in the semiconductor, and hence maximum electric field is limited to twice the intrinsic

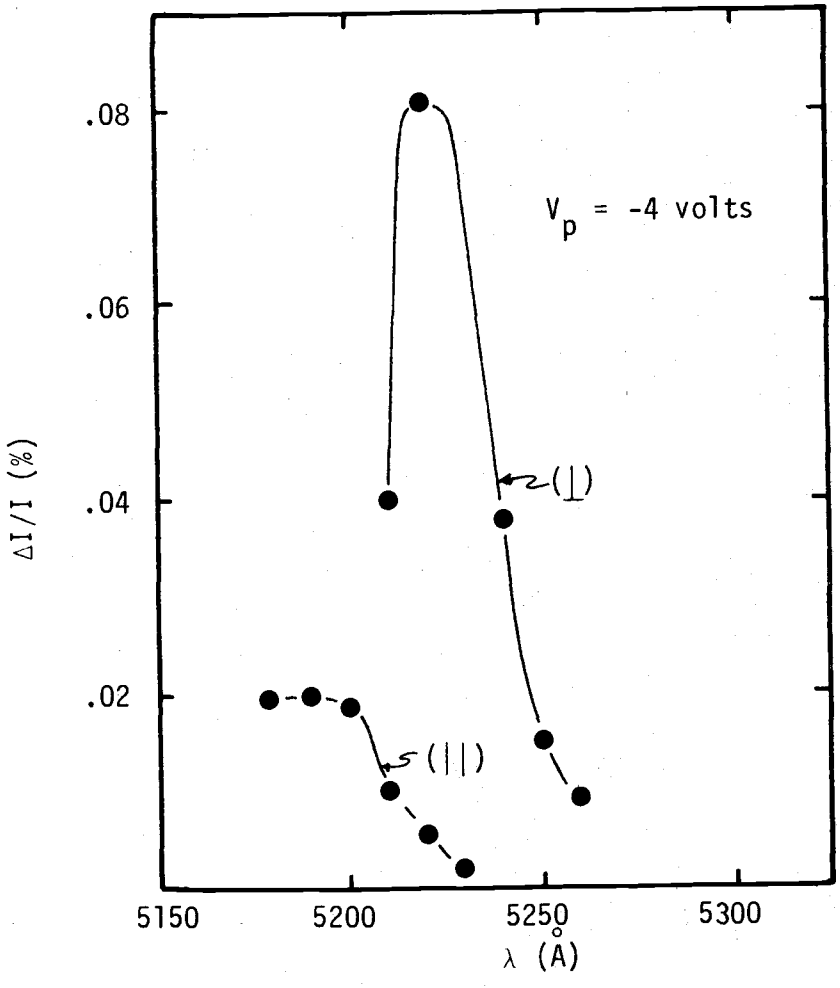

Figure 27. Percentage intensity change for MIS 2 with polarized incident light.

Fermi level (14). High d-c fields are not possible unless the semiconductor is very highly-doped. A decrease in depletion width would result.

(2) Metal-Semiconductor Barrier Diodes

Figure 28 shows the relative transmitted intensity (normalized to 100 percent) spectra for the metal-semiconductor barrier devices. The spectra for two polarizations are also illustrated. Again, it is shown that the edges are separated by approximately 40 Å.

The active areas of the devices are 44.2×10^{-4} in.^{2} (.075" diameter). The Au film is 10Ω/□ for device #1 and 1870 Ω/□ for device #2. The difference in Au film thickness account for the observed differences in transmitted intensity levels of the devices.

The $\Delta I/I$ percentage as a function of wave length for several applied voltages on SBL 1 is shown in Figure 29. The incident light is unpolarized and the current through the sample during the bias cycle is less than 50 μA. Thus, heating of the sample does not occur (see Appendix III).

For incident light wave length λ = 5240 Å, the change in transmitted intensity ΔI (relative units) is observed to be proportional to the square of the applied voltage, implying the ΔI is proportional to E_m^4 (see Figure 30). This behavior is different from that of the MIS diodes in which ΔI is proportional to the square of E_m.

The variation of $\Delta I/I$ spectra of SBL 2 is shown on Figure 31 for an applied voltage of 4 volts and current < 100 μA. For the unpolarized case, $\Delta I/I$ of SBL 2 is of the same magnitude as $\Delta I/I$ of SBL 1 with less than 3 volts applied. This difference may be due to

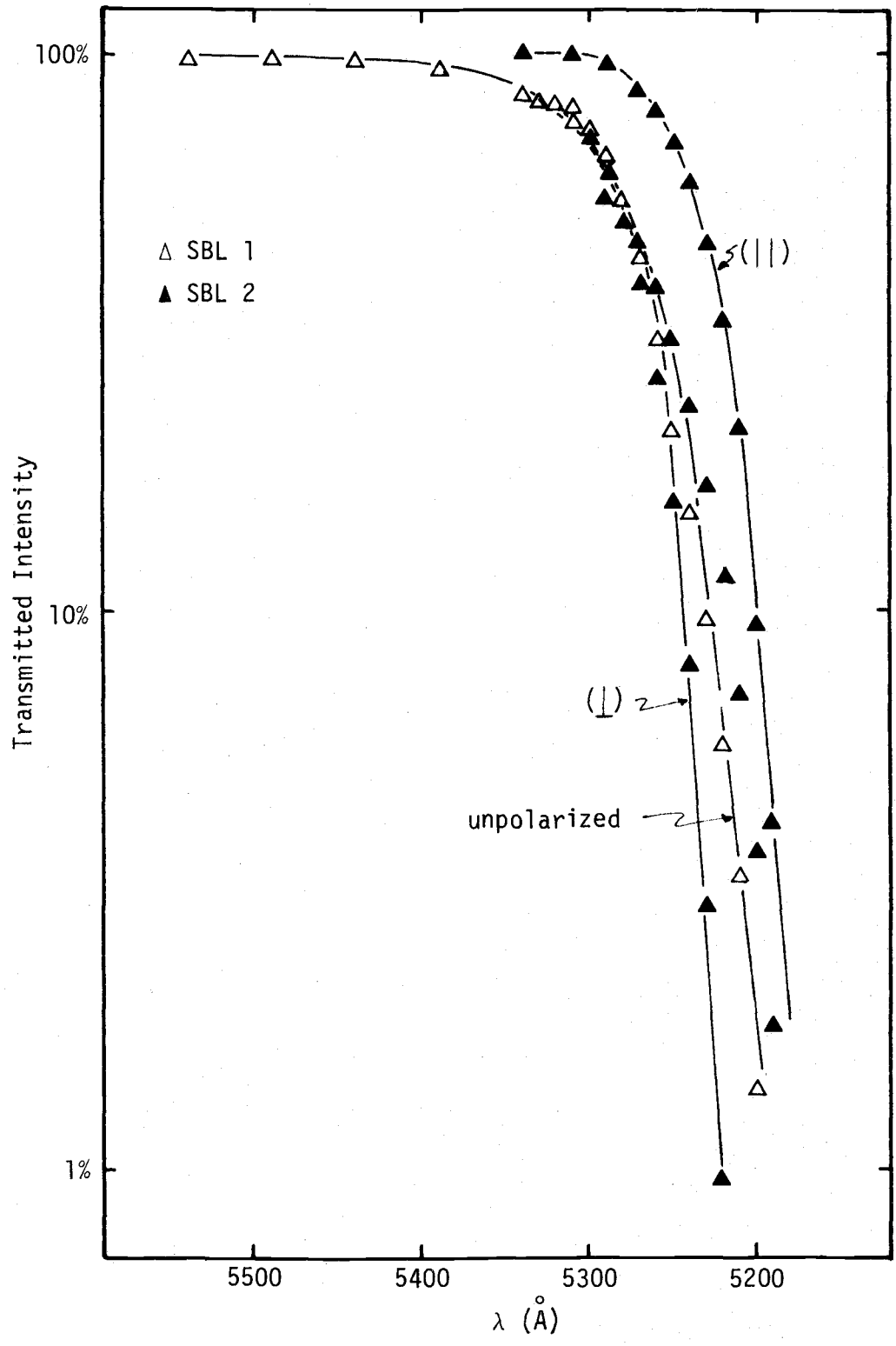

Figure 28. Transmitted intensity spectra for SBL 1 and SBL 2.

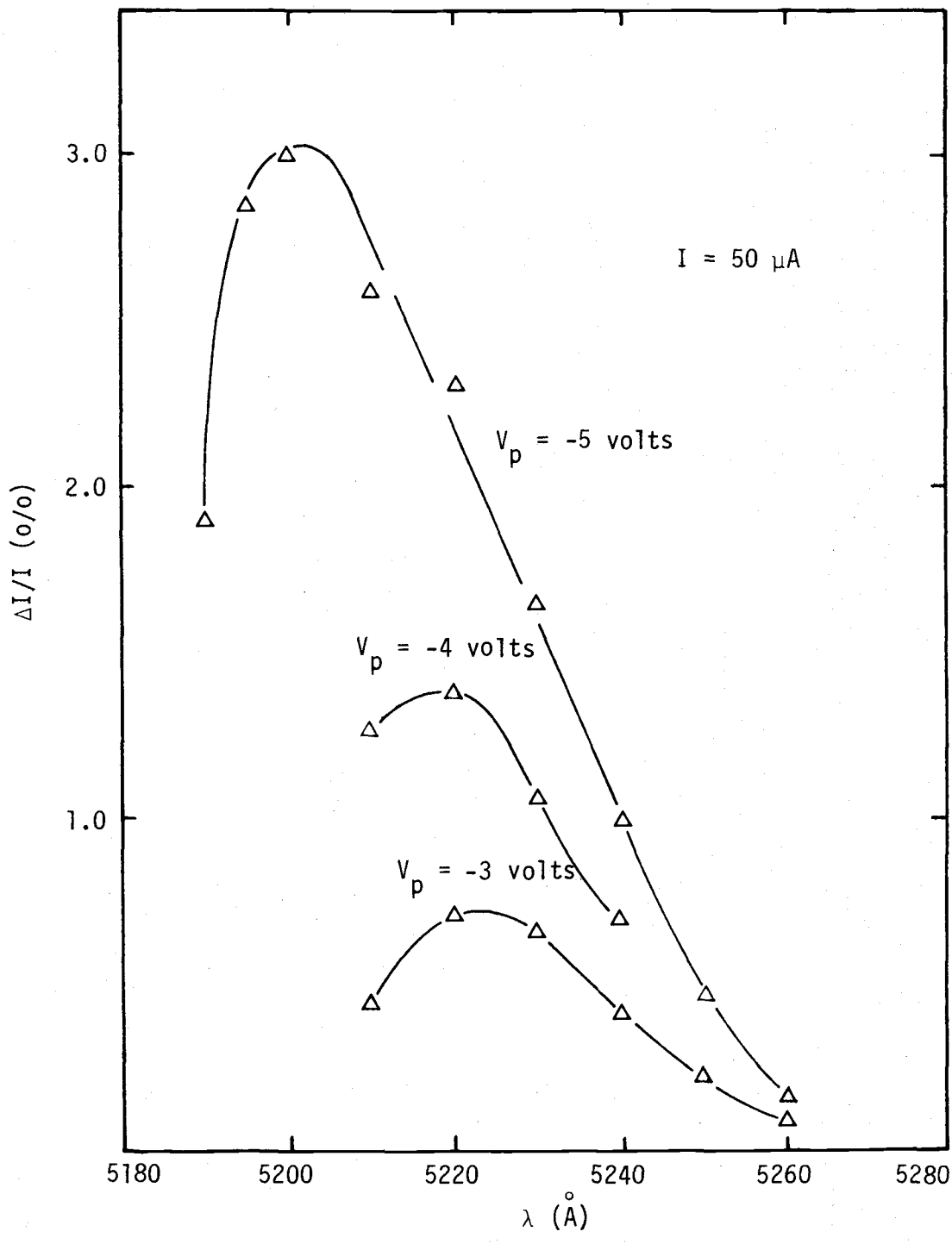

Figure 29. Percentage intensity change for SBL 1 with unpolarized incident light.

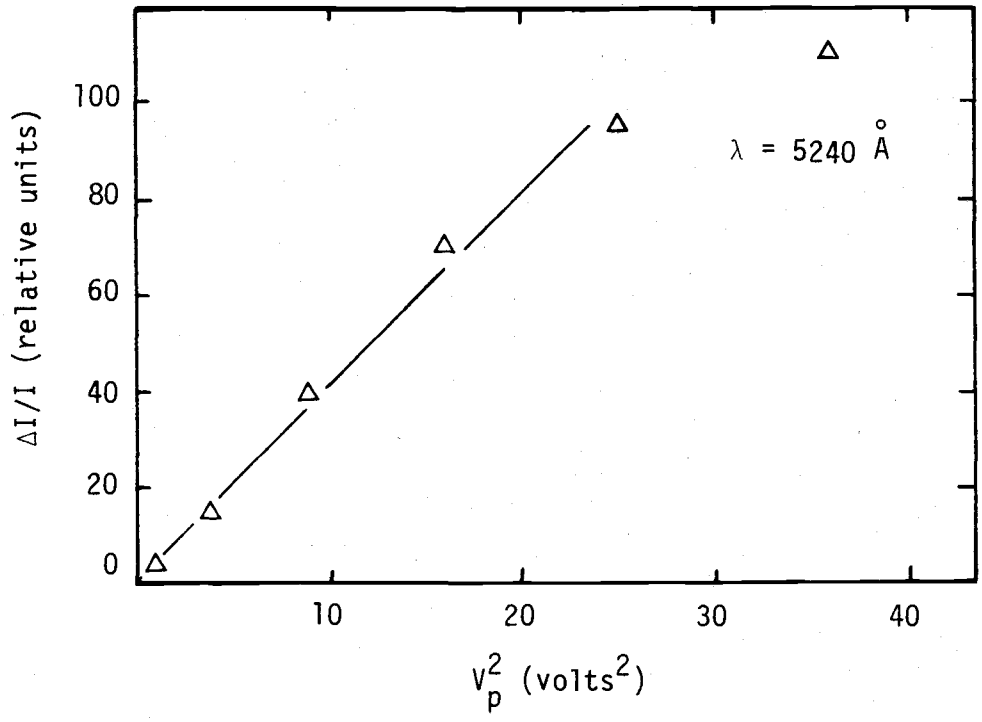

Figure 30. Relative intensity change with the square of applied voltage on SBL 1.

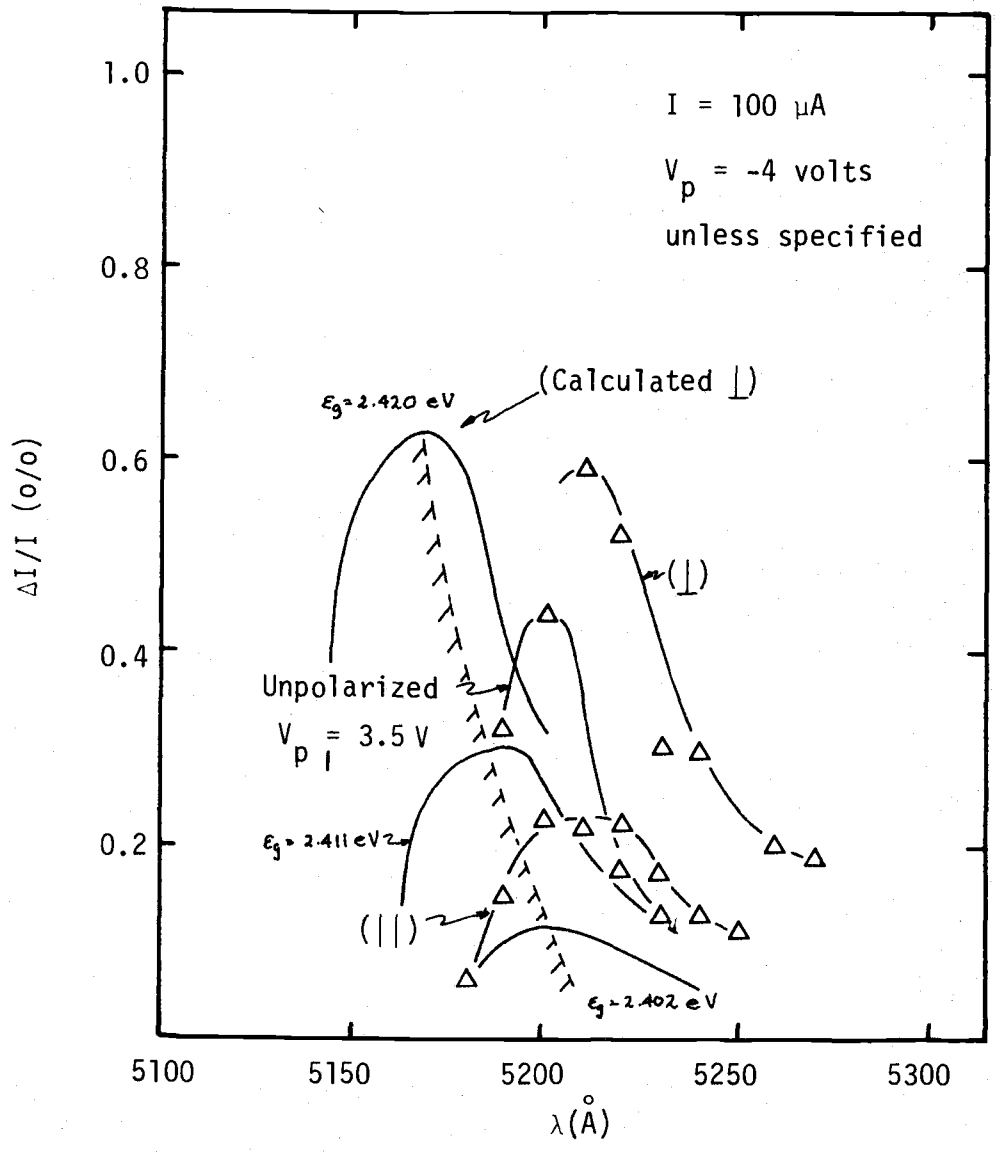

Figure 31. Percentage intensity change for SBL 2 with polarized and unpolarized incident light.

the difference in Au film thickness of the barrier electrode. In SBL 2 the sheet resistance of the Au film is approximately 180x that of device SBL 1. The higher sheet resistance of the electrode causes more voltage to be dropped across it and decreases the voltage across the diode space-charge region. Shown also in Figure 31 is the transmitted intensity of SBL 2 for both parallel and perpendicularly polarized incident light. The parallel polarization spectrum again is broad and flat compared to the perpendicularly polarized spectrum.

The bandwidth of SBL 1 decreases from 43 Å to 30 Å as the voltage decreases from 5 volts to 3 volts; the incident light being unpolarized. The bandwidth of SBL 2 is 30 Å for an applied voltage of 3.5 volts and unpolarized incident light. It is difficult to say what the bandwidth of SBL 2 is with perpendicularly polarized incident light due to a missing data point. For parallel polarized light incident on SBL 2 the bandwidth is 50 Å with an applied voltage of 4 volts.

It was thought that if the resistivity of the semiconductor was increased and hence the depletion region increased, a larger percentage of $\Delta I/I$ could be obtained assuming the same field was applied. Therefore, two samples were fabricated using $10^6 \Omega$ -cm (dark resistivity) material whose c- axis was perpendicular to the major face. The active areas were 0.075 in. in diameter. The thickness of the Au film was 43 Ω/□ and 10 Ω/□ on SBH 1 and SBH 2, respectively.

The transmitted intensity spectra for both devices are shown in Figure 32. We noted in this case, that they are nearly the same magnitude confirming that the Au film thicknesses are the same, since the CdS thicknesses are identical.

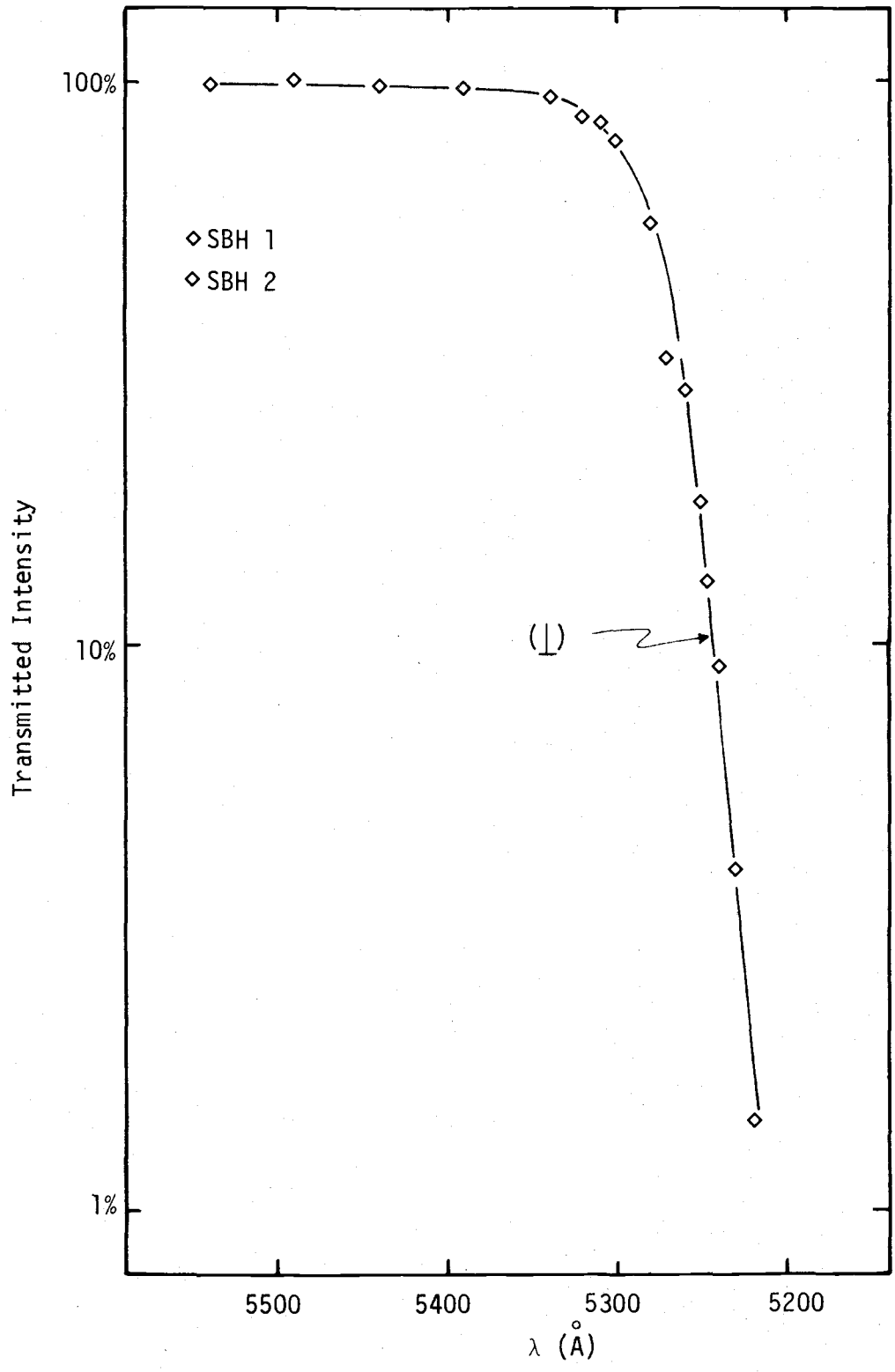

Figure 32. Transmitted intensity spectra for SBH 1 and SBH 2.

Illustrated in Figure 33 are the percentage changes in transmitted light spectra for both SBH 1 and SBH 2. The applied voltage is 80 volts for both; a 60 volt spectrum is also shown for SBH 1. The currents are kept to values below 50 μA for SBH 1 and 10 μA for SBH 2. The maximum values of $\Delta I/I$ are less than one percent and the peaks are separated by only 10 Å (monochromator limit).

The I-V characteristics of the devices shown in Figure 34 indicate that the indium contact to CdS is not exactly ohmic. This would increase the zero-bias absorption and the percentage intensity change altered.

The variation of $\Delta I/I$ (relative units) with applied voltage is shown in Figure 35 for both SBH 1 and SBH 2; λ = 5230 Å for SBH 1 and 5220 Å for SBH 2. We observe that contrary to the SBL case, the relation between $\Delta I/I$ and V_a is a linear one, implying that $\Delta I/I$ is proportional to E_m^2. This behavior is similar to that observed in the MIS diodes.

The bandwidths of the SBH devices are 40 Å for 80 volts and 25 Å for 60 volts. These values are for perpendicularly polarized incident light on the sample.

The advantage of the SBL configuration is that all of the applied voltage appears across the space charge region, i.e., efficient use of applied voltage, d-c reverse biases corresponding to the breakdown field of the material could be applied. The disadvantage is that the edge breakdown and high currents usually preceeds the material breakdown. In the SBH configuration wide space-charge regions are possible but requires larger voltages. Ohmic contact to the semiconductor are

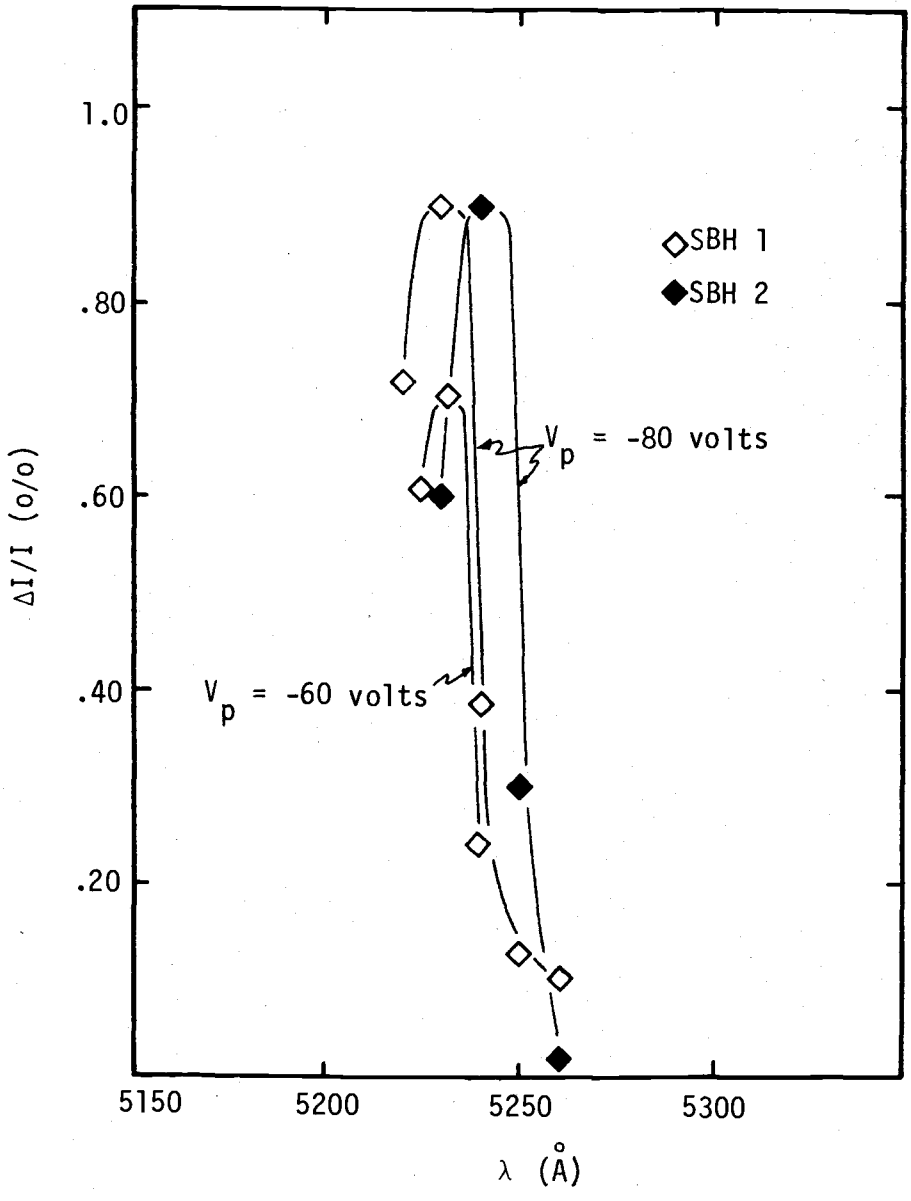

Figure 33. Percentage intensity change for SBH 1 and SBH 2.

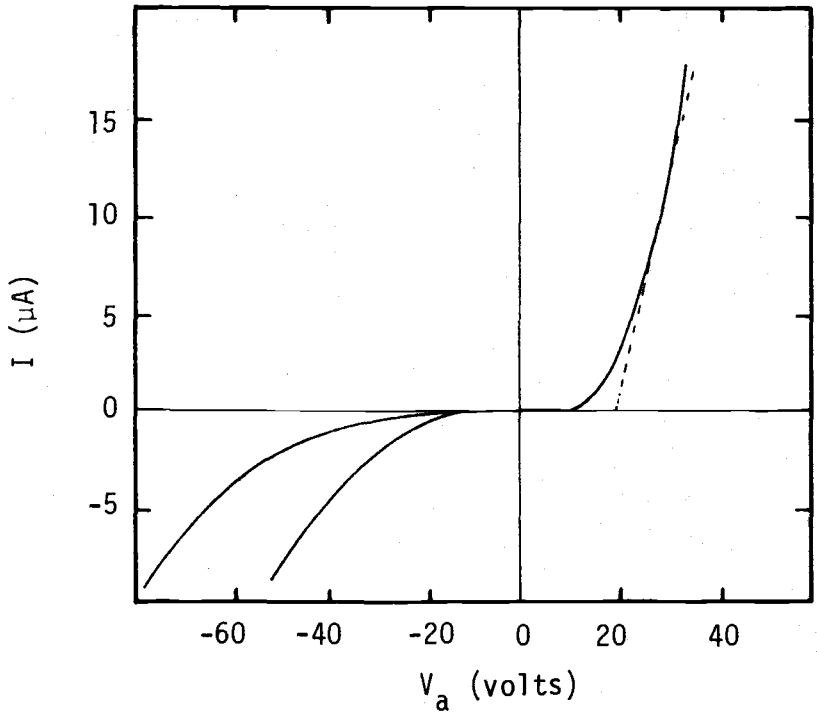

Figure 34. Current-voltage characteristics of SBH 1 and SBH 2.

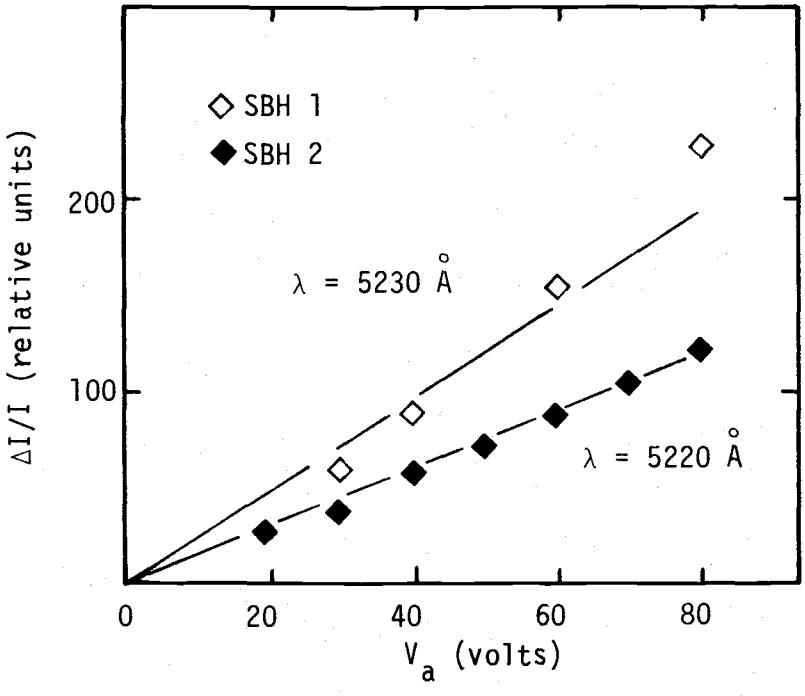

Figure 35. Relative intensity change with applied voltage on SBH 1 and SBH 2.

more difficult to obtain with high resistivity material. Hence, some of the applied voltage will appear across the non-ohmic contact.

(3) P-N Heterojunction Diodes

The transmitted intensity spectra of samples PN 1 and 2 are shown in Figure 36. The parallel and perpendicular polarization spectra of PN 1 are separated by approximately 35 Å, as expected. The relative magnitudes of the unpolarized spectra of PN 1 and PN 2 are the same, indicating the same thickness of CdS and Cu_xS layers.

The active areas of the junction are .075 inch in diameter and the depth of the p-region is estimated to be 5000 Å. The absorption coefficient of the Cu_xS layer is assumed to be constant and independent of applied field in the light frequencies near the CdS band edge.

Illustrated in Figure 37 are the $\Delta I/I$ spectra for PN 1 and PN 2 with unpolarized incident light. The orders of magnitude of $\Delta I/I$ are comparable to those observed in the previous samples, i.e., MIS 1 and 2, SBL 1 and 2. Within experimental error the peaks occur at the same wave length as the previous samples of differing configurations. The current was kept below 4 μA at an applied voltage of 10 volts in PN 2.

With unpolarized incident light, $\Delta I/I$ is observed to vary as the square of the applied voltage at λ = 5210 Å (see Figure 38). This behavior is similar to that observed in the SBL 1 and SBL 2 samples. Once again such a variation of $\Delta I/I$ with applied voltage implies that $\Delta I/I$ varies as E_m^n where n = 4.

For an applied voltage of ten volts the bandwidth of PN 1 is 70 Å and 40 Å for an applied voltage of six volts as illustrated in Figure 39. With perpendicularly polarized light incident on the

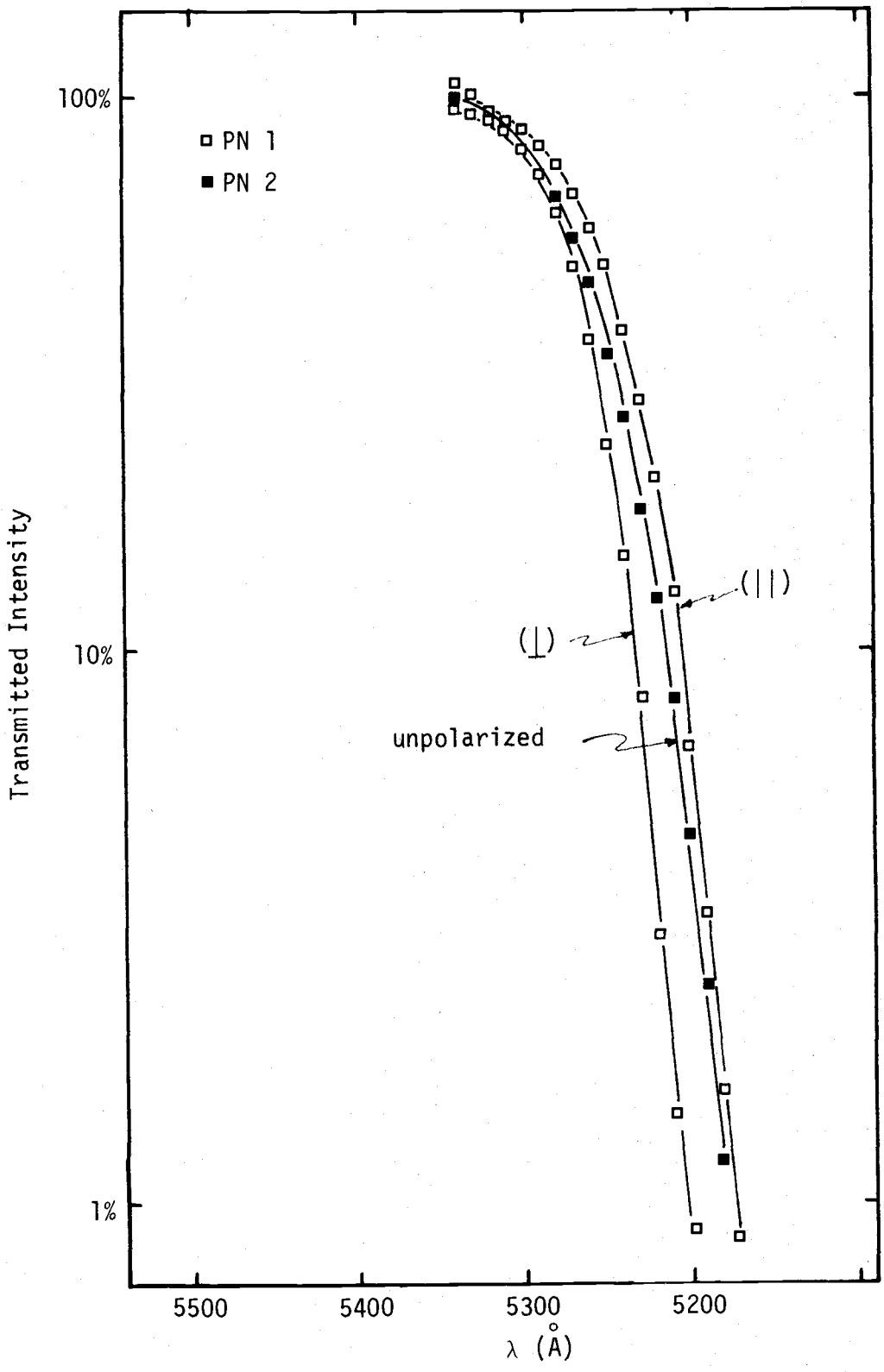

Figure 36. Transmitted intensity spectra for PN 1 and PN 2.

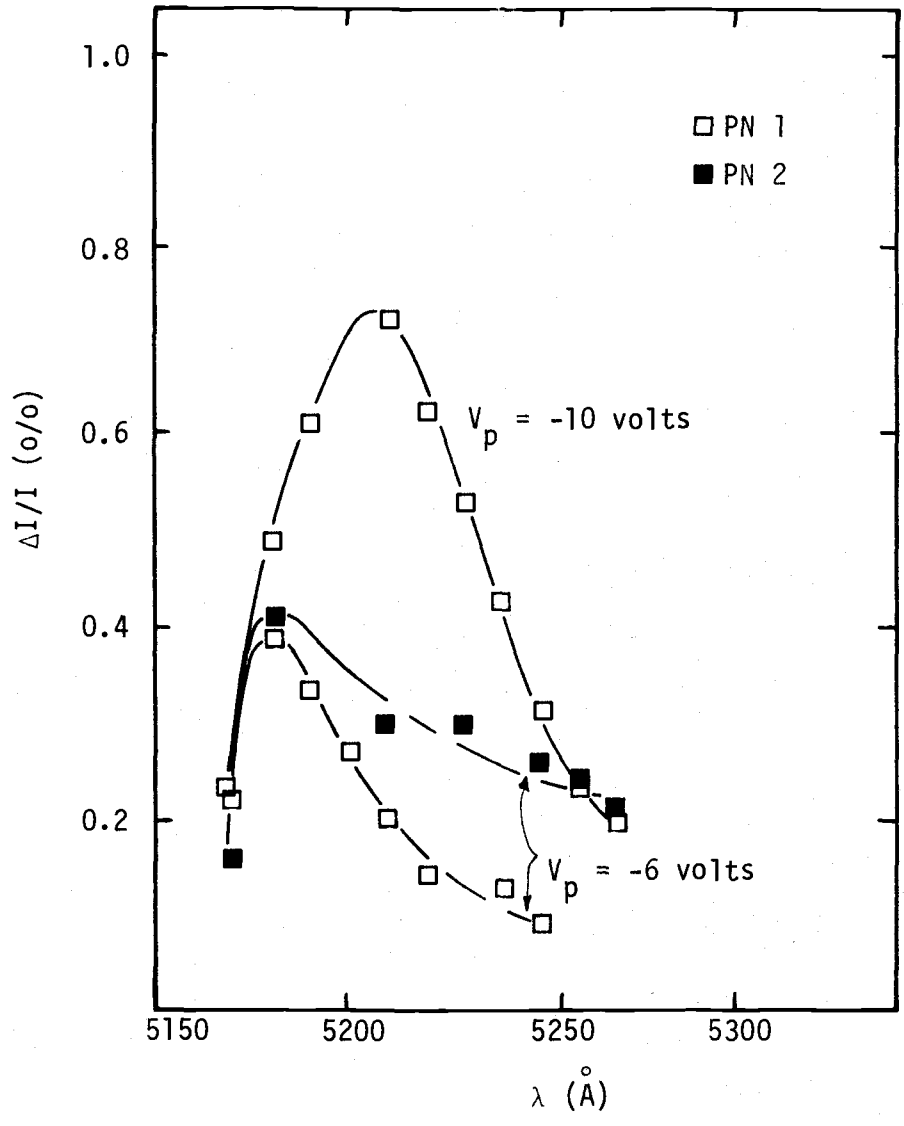

Figure 37. Percentage intensity change for PN 1 and PN 2 with unpolarized incident light.

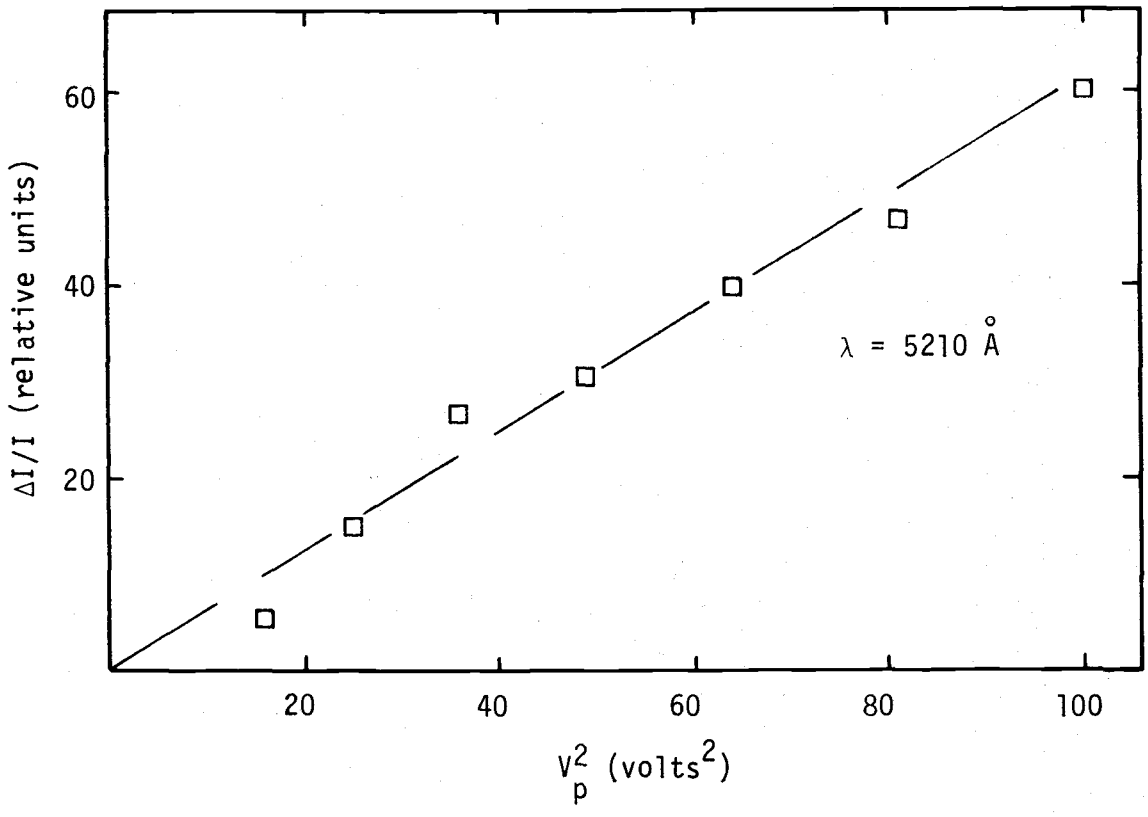

Figure 38. Relative intensity change with the square of applied voltage on PN 1.

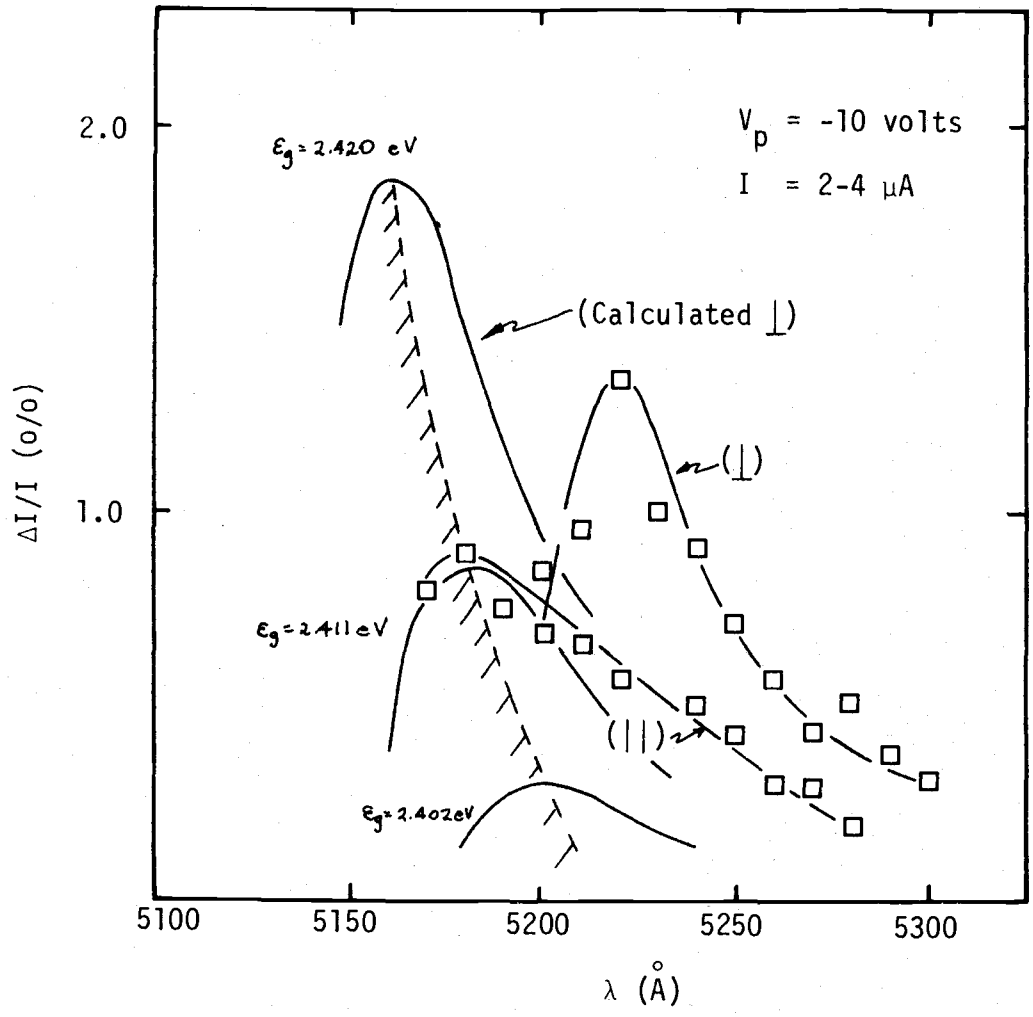

Figure 39. Percentage intensity change for PN 1 with polarized incident light.

sample the bandwidth is 45 Å for an applied voltage of ten volts. The device bandwidth appears slightly wider for the parallel polarized incident light.

The advantages of this diode configuration are the same as those of the metal-semiconductor barrier providing the p-region remains shallow and heavily doped; i.e., minimum voltage drop across the p-region. With our equipment, the thickness of this region is more easily controlled than the thickness of the gold film. Since the junction is below the surface, the device characteristics are less dependent upon the surface conditions. The problem of edge breakdown, however, is still present in this type of configuration, i.e., p^+-n junction.

Comparison of Results with Expectations

Qualitatively the results seem to be in accordance to what was expected. The magnitude of the peaks increased with voltage. The shape of the $\Delta I/I$ curves are similar to the theoretical curves. The energy bandwidth of the intensity changes are approximately 40 to 50 Å as predicted and bandwidth increases with increasing applied voltages.

In the uniform electric field case, $\Delta\alpha/\alpha$ is proportional to exp (E^2), the relationship being simple. In the linear electric field case, $\Delta I/I$ is not a simple function of E_m and comparison with experimental curves would be difficult. If $\Delta\alpha_{eff}\ \Delta W$ is small, we can say

$$\Delta I/I \quad - \Delta\alpha_{eff}\ \Delta W \text{ and}$$

if KE_m is small, which is true for energies below the peak then,

$$\Delta\alpha_{eff} = \frac{KE_m}{2}\,\alpha_o$$

$$\frac{\Delta I}{I} = \frac{KE_m}{2}\,\Delta W\,\alpha_o \tag{6.1}$$

But W is proportional to E_m. Hence,

$$\frac{\Delta I}{I} \sim E_m^{\,2} \tag{6.2}$$

which is the behavior observed in both the MIS and SBH samples.

We will now attempt to see if our experimental results are quantitatively similar to the curves which are generated with the equations in Chapter III. In order to arrive at the calculated curves in Figure 31 and Figure 39, we used the absorption coefficient values in (6). The reason for doing this is two-fold: (a) the crystal thickness is too large to allow transmission measurements below 5150 Å and (b) the monochromator resolution is only 10 Å which would prevent accurate determinations of α.

In both of the figures, we have shown calculated curves based on three choices of energy gap. The curves define a shaded region in which the experimental results may be expected. This shaded region may be shifted horizontally by using the absorption spectra of others.

The values of E_m for diode SBL 2 are computed for $V_a = 0$ and $V_a = 4$ volts. Assuming a built-in voltage of 0.7 volt (see Ref. 31), E_m is calculated to be 2.4×10^4 V/cm and 6×10^4 V/cm for applied voltages of zero and four, respectively (see Appendix II). The corresponding depletion widths are computed as 0.57 micron and 1.50 microns; the increase in space-charge region being 0.93 microns. Since the product of $\Delta\alpha_{eff}$ and $\Delta W << 1$, we can safely say that the quantity $\Delta I/I$ is proportional to $\Delta\alpha_{eff}\,\Delta W$ which is plotted in Figure 31.

In order to obtain the calculated curves in Figure 39 for perpendicular polarization, we assume an abrupt p^+-n junction, i.e., the applied voltage appears mostly in the CdS region. The change in depletion width is calculated to be 1.71 micron and E_m equal to 9.5×10^4 V/cm for an applied voltage of 10 volts (see Appendix II). The $\Delta\alpha_{eff}\,\Delta W$ product is small (< five percent at maximum); so we can safely assume that $\Delta I/I$ is proportional to $\Delta\alpha_{eff}\,\Delta W$.

We see that the magnitudes are approximately the same for both calculated and experimental curves but the peaks differ slightly. If the peaks are matched, the magnitudes are no longer the same. These difficulties were very similar to those encountered by others (22,1). Our deviations are in $\Delta I/I$ whereas Lambert (22) and others have reported deviations in α which would make deviations in $\Delta I/I$ worse than our case.

VII. CONCLUSIONS AND SUGGESTIONS

An expression for the change in transmitted light intensity has been developed for devices in which the electric field varies linearly with distance. The expression is in terms of the maximum value of the electric field and derived from the one-electron calculations of Franz. The difficulties in obtaining reasonable matches of experimental results and theoretical predictions are illustrated. One of the reasons for this is that the theory of Franz is too simple.

The $\Delta I/I$ percentage of the rest of the devices were on the order of one percent for relatively low maximum electric fields ($\simeq 5 \times 10^4$ V/cm). Large changes in transmitted light intensities are predicted by our expression for higher values of electric field, i.e., greater than 2×10^5 V/cm. $\Delta I/I$ is observed experimentally to be proportional to either E_m^2 or E_m^4. Hence, the use of these diodes to control the intensity of the light source is feasible if devices with high electric fields could be fabricated. We encountered insurmountable difficulties in attempting to fabricate devices which had low reverse leakage currents at high electric fields. The problem here is still one of technology.

We have observed field-induced absorption in two configurations of CdS not reported previously. These configurations are the Schottky barrier and the p^+-n heterojunction. These configurations could be used by others who would be interested in determining the physical properties of CdS.

By using the differential method, of measuring the change in transmitted intensities we have avoided the problem of overheating in

the samples, which has not been mentioned in several articles where large changes in transmission were reported (1,20). It is suspected that much of the change is due mainly to heating and not the electric field.

Since the acquisition of relatively high electric fields is the biggest problem, the following suggestions are aimed towards that end.

(1) Make the active areas smaller so that the chances of imperfections are decreased. Larger uniform areas are also difficult to obtain.

(2) Perhaps decrease the edge leakage of the Au-CdS diodes by the incorporation of a guard ring, as shown in Figure 40. A similar technique is used in the fabrication of Schottky barrier avalanche photo-diodes (23).

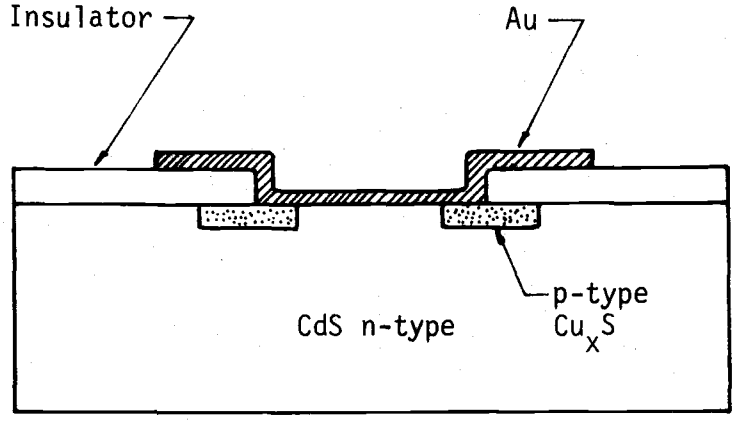

Figure 40. Au-CdS barrier diode with guard ring.

BIBLIOGRAPHY

1. Boer, K. et al. Anwendung elektro-optischer Effekte zur Analyse des elektrischen Leitungs vorganges in CdS-Einkristallen Zietschrift für Physik 155:170. 1959.

2. Bube, R. and Gill, W. Photovoltaic Properties of Cu_2S-CdS Heterojunctions. Journal of Applied Physics 41:3731. 1970.

3. Callaway, J. Optical Absorption in an Electric Field. Physical Review 130:549. 1963.

4. _____. Optical Absorption in an Electric Field. Physical Review 134:A998. 1964.

5. Chester, M. and Fritsche. Phonon-Assisted Electroabsorption. Physical Review 139:A518. 1965.

6. Dutton, D. Fundamental Absorption Edge in CdS. Physical Review 112:785. 1958.

7. Eden, R. and Coleman, P. Proposal for Microwave Modulation of Light Employing the Shift of Optical Absorption Edge with Applied Electric Field. Proceedings of the Institute of Electrical and Electronic Engineers 53:1776. 1963.

8. Elliott, R. Intensity of Optical Absorption by Excitons. Physical Review 108:1387. 1957.

9. Franz, W. Einfluss eines electrischen Feldes auf eine optische Absorptionskante. Zietschrift für Naturforschung 13a:484. 1958.

10. French, B. Effect of a Uniform Electric Field Upon the Optical Absorption of Semi-Insulating Gallium Arsenide. Physical Review 174:991. 1968.

11. Frova, A. and Handler, P. Shift of Optical Absorption Edge by and Electric Field: Modulation of Light in the Space-Charge Region of a Ge p-n Junction. Applied Physics Letters 5:11. 1964.

12. _____. Franz-Keldysh Effect in the Space-Charge Region of a Germanium P-N Junction. Physical Review Letters 137:A1857. 1965.

13. _____. Direct Observations of Phonons in Silicon by Electric Field-Modulated Optical Absorption. Physical Review Letters 14:178. 1965.

14. Grove, A. Physics and Technology of Semiconductor Devices. New York, John Wiley and Sons, Inc., 1967. 366 p.

15. Geutsche, E. and Lange, H. Determination of Effective Mass from Field-Induced Shift of Absorption Edge. In: Physics of Semiconductors. Proceedings of 7th International Conference. Paris. 1964.

16. _____. Field Induced Shift in the Absorption Edge in CdS. Physica Status Solidi 4:K21. 1964.

17. Heilmeir, G., Zanoni, L. and Barton, L. Dynamic Scattering: A New Electrooptic Effect in Certain Classes of Nematic Liquid Crystals. Proceedings of the Institute of Electrical and Electronic Engineers 56:1162. 1968.

18. Heilmeir, G., Castellano, J. and Zanoni, L. Guest-Host Interactions in Nematic Liquid Crystals. Molecular Crystals and Liquid Crystals 8:293. 1969.

19. Heilmeir, G. and Goldmacher, J. A New Electric Field Controlled Reflective Optical Storage Effect in Mixed Liquid Crystal Systems. Proceedings of the Institute of Electrical and Electronic Engineers 57:34. 1969.

20. Honda, M., Fujimori, M. and Nishimura, Y. Light Intensity Modulation in CdS Film by Franz-Keldysh Effect. In: Integrated Optics--Guided Waves, Materials and Devices. Las Vegas. 1972. p. WB1-1.

21. Keldysh, L. The Effect of a Strong Electric Field on the Optical Properties of Insulating Crystals. Soviet Physics JETP 34:788. 1958.

22. Lambert, L. Measurement of Optical Absorption in an Electric Field. Physical Review 138:A1569. 1965.

23. Lepselter, M. and Sze, S. Near-Ideal Metal-Semiconductor Barriers. Institute of Electrical and Electronic Engineers Transactions on Electron Devices ED-15:434. 1968.

24. Milnes, A. and Feucht, D. Heterojunctions and Metal-Semiconductor Junctions. New York, Academic Press, 1972. 408 p.

25. Moss, T. Optical Absorption Edge in GaAs and its Dependence on Electric Field. Journal of Applied Physics 32:2136. 1961.

26. Okazaki, S. and Otaki, E. Properties of Intersurface in Au-insulator-CdS Measured by Capacitance Method. Japanese Journal of Applied Physics 5:181. 1966.

27. Penchina, C. Phonon-Assisted Optical Absorption in an Electric Field. Physical Review 138:A924. 1965.

28. Perov, P. et al. Effect of Strong Electric Field in Exciton Absorption Lines in Some Films. Journal of Vacuum Science and Technology 6:753. 1969.

29. _____. Effect of a Strong Electric Field on CdS Exciton Absorption. Soviet Physics-Solid State 11:65. 1969.

30. Racette, G. Absorption Edge Modulator Utilizing a P-N Junction. Proceedings of the Institute of Electrical and Electronics Engineers 52:716. 1964.

31. Spitzer, W. and Mead, C. Barrier Height Studies of Metal--Semiconductor Systems. Journal of Applied Physics 34:3061. 1963.

32. Tharmalingham, K. Optical Absorption in the Presence of a Uniform Field. Physical Review 130:2204. 1963.

33. Vavilov, V. and Britsyn, K. The Effect of Strong Electric Field on the Absorption of Light by Silicon. Soviet Physics-Solid State 2:1746. 1964.

34. Wang, S. Solid State Electronics. New York, McGraw-Hill, 1966. 778 p.

35. Weast, R. (ed.). Handbook of Chemistry and Physics. Cleveland, The Chemical Rubber Co., 1969.

36. Williams, R. Electric Field Induced Light Absorption in CdS. Physical Review 117:1487. 1960.

37. _____. Effect of High Electric Field on the Absorption of Light by PbI_2 and HgI_2. Physical Review 126:442. 1962.

38. Yacoby, Y. Electric-Field-Induced Optical Absorption in Solids and the Fine Structure of the Stark Splitting. Physical Review 140:A263. 1965.

39. Zettler, R. and Crowley, A. P-N Junction-Schottky Barrier Hybrid Diode. Institute of Electrical and Electronic Engineers. Transactions on Electron Devices ED-16:58. 1969.

APPENDICES

APPENDIX I

Step by Step Fabrication Procedure of Devices

(1) MIS

(a) Mounted crystal on lapping block with black Apiezon wax (see Figure A.1).

(b) Polished crystal with 0.5μm CR_2O_3 paper until smooth as observed under 100x magnification of microscope.

(c) Turned crystal over and polished other side on which device will be made.

(d) Crystal removed from lapping block and boiled in acetone to remove the wax.

(e) Rinse in DI H_2O.

(f) Etched in 10:1 HCL for 30 sec.

(g) Rinse in DI H_2O and blow dry with N_2.

(h) Stick in high vacuum system.

(i) Deposit Al_2O_3
Evaporation conditions for #1
Starting pressure = 4×10^{-6} torr
Ending Pressure = 10^{-5} torr
Substrate Temperature = room temperature
Δf (thickness monitor) = 900 Hz
e-gun current = 60-80 m A
evaporation time = 10' 10"
Evaporation conditions for #2
Starting Pressure = 2×10^{-6} torr
Ending Pressure = 4×10^{-5} torr
Substrate Temperature = room temperature
Δf (thickness monitor) = 1050 Hz
e-gun current = 90-115 m A
evaporation time = 10' 00"

(j) remove from high vacuum system and place foil mask on sample.

(k) Deposit Au top electrode using Al_2O_3-coated W basket
Evaporation conditions for #1
pressure $\leq$ 0.1 micron
substrate temperature = room (25°C)

filament current = 18 A
evaporation time = 19 sec.
Evaporation conditions for #2
pressure $\leq$ 0.1 micron
substrate temperature = room (25°C)
filament current = 20 A
evaporation time = 10 sec.
Sheet resistance = 525 Ω/□

(l) remove from diffusion pump system and mount on holder (see Figure A.1).

(m) use silver print to connect .002 Au wire to Au electrode.

(2) Metal-Semiconductor Barrier

Steps (a) to (e) are similar to those in section 1.

(f) mount sample on .2 cm x .2 cm glass slide using wax.

(g) rinse in DI H_2O and blow dry with dry N_2.

(h) mount on spinner and apply photoresist (Kodak AZ 1350).

(i) spin at #7 on potentiometer. (Platt spinner)

(j) dry photoresist in chamber at 60°C and -20 in. for 10 min.

(k) expose photoresist using available Kodak high resolution emulsion masks - 4 second exposure.

(l) the photoresist is developed with Kodak developer--30 seconds in developing solution.

(m) rinse in DI H_2O and blow dry with N_2.

(n) examine pattern with microscope (50x magnification) to insure good patterns.

(o) heat sample to 150°C for 3 minutes with hot plate.

(p) remove sample from glass slide.

(q) rinse wax off sample with TCE.

(r) etch in 10:1 HCl for 30 seconds.

(s) rinse with DI H_2O and blow dry with N_2.

(t) mount crystal on holder and place foil mask over sample.

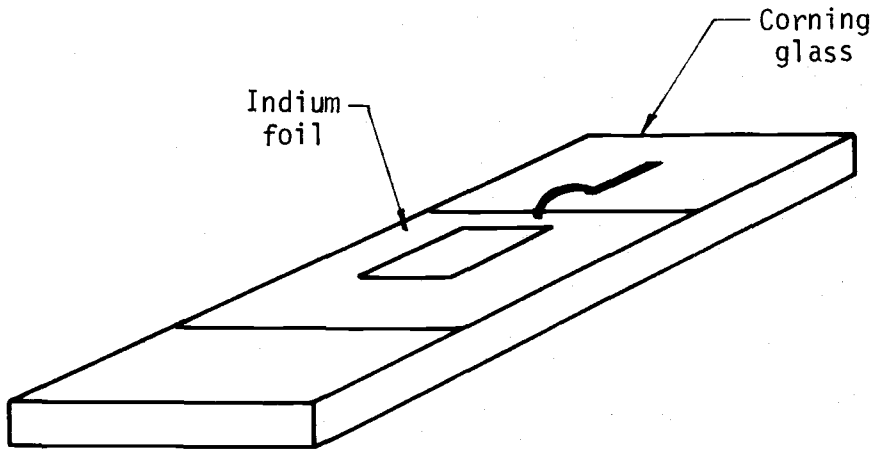

Figure A1. Sample mounts.

(u) Deposit Au top electrode using tungsten filament.
Evaporation conditions for SBL #1
pressure $\leq$ 0.1 micron
substrate temperature = room (25°C)
filament current = 50 A
evaporation time = 4 sec.
sheet resistance = 10 Ω/□
Evaporation conditions for SBL #2
pressure $\leq$ 0.1 micron
substrate temperature = room (25°C)
filament current = 19 A (Al_2O_3) coat W basket)
evaporation time = 10 sec
sheet resistance = 1870 Ω/□

(v) connect .002" Au wire to Au electrode with silver print.

(3) P-N Heterojunction

Steps (a) through (o) are the same as those in section 2.

(p) while sample is still on hot plate use black wax to cover the sides of the crystal.

(q) dip sample in solution containing:

80ml DI H_2O
0.5 g CuCl
a minute amount of hydroxlaminehydrochloride and a drop of concentrated HCl acid.

for five minutes at 80°C.

(r) rinse with DI H_2O and blow dry with N_2.

(s) remove sample from glass slide by heating to 150°C.

(t) wash wax off sample by rinsing in toluene.

(u) rinse with DI H_2O and blow dry with N_2.

(v) heat sample to 250°C for one minute in air.

(w) mount sample on holder and attach Au lead to p-type with silver print.

APPENDIX II

Computation of Maximum Electric Fields and Depletion Widths for Diodes

(1) MIS Diode

$$W = \left[\frac{2\varepsilon_s}{qN_D} V_T \right]^{1/2}$$

$$E_{max} = \frac{q N_D W}{\varepsilon_s}$$

where $V_T = V_b + V_a$

V_T is total voltage across the space charge region

V_a is applied voltage

V_b is reported to be 1.00 volt for etched surfaces (26).

$$\varepsilon_s = 8.86 \qquad \rho = 10\Omega\text{-cm}$$

For $V_a = 0$

$$W = \left[\frac{2\varepsilon_s}{qN_D} V_b \right]^{1/2} = \left[\frac{2 \times 8.64 \times 8.84 \times 10^{-14}}{1.6 \times 10^{-19} \times 2 \times 10^{15}} \right]^{1/2} V_b^{1/2}$$

$$= 6.91 \times 10^{-5} \text{ cm} = .69 \text{ micron}$$

Because we are applying a voltage at 400Hz, most of the applied voltage (4 volts) appears across the space charge region. Now,

$$W = \left[\frac{2\varepsilon_s}{qN_D} V_T \right]^{1/2} = 6.91 \times 10^{-5} (4.5)^{1/2}$$

$$W = \left[\frac{2\varepsilon_s}{qN_D} V_T\right]^{1/2} = 6.91 \times 10^{-5} (4.5)^{1/2}$$

$$= 1.47 \times 10^{-5} = 1.47 \times 10^{-5} = 1.47 \text{ microns}$$

and

$$E_{max} = .042 \times 10^{10} \times 1.47 \times 10^{-4} = 6.19 \times 10^{4} \text{ v/cm.}$$

$$\Delta W = 1.47 - .69 = .78 \text{ micron}$$

(2) Metal-Semiconductor Barrier Diode

$$W = \left[\frac{2\varepsilon_s}{qN_D} (V_b - V_a - \frac{kT}{q})\right]^{1/2}$$

$$E_{max} = \frac{qN_D W}{\varepsilon_s} = \left[\frac{2qN_D}{\varepsilon_s} (V_b - V_a - \frac{kT}{q})\right]^{1/2}$$

$$V_b = \Delta\phi - \zeta$$

where

$$\Delta\phi = \phi m - \chi_s = 0.80 \text{ eV for CdS (31)}$$

and

$$\zeta = (E_c - E_f) = .10 \text{ eV (31)}$$

For $V_a = 0$, $\rho = 10\Omega$ -cm

$$W = 6.91 \times 10^{-5} V_b^{1/2} = 6.91 \times 10^{-5} (0.675)^{1/2} = 5.7 \times 10^{-5} \text{ cm}$$

$$= .57 \text{ micron}$$

For V_a = -4 volts

$$W = 6.91 \times 10^{-5} (4.675)^{1/2} = 1.5 \times 10^{-4} \text{ cm}$$

$$= 1.5 \text{ micron}$$

$$E_{max} = .042 \times 10^{10} (1.5 \times 10^{-4}) = 6.3 \times 10^{4} \text{ V/cm}$$

$$W = 0.93 \text{ micron}$$

For V_a = 0, $\rho = 10^6 \Omega$ -cm (dark)

$$W = 6.91 \times 10^{-3} (V_b)^{1/2}$$

$$V_b = \Delta\phi - \zeta$$

$$\Delta\phi = 0.8, \zeta = 0.4 \text{ eV (calculated)}$$

$$V_b = 0.4 \text{ volt}$$

$$W = 6.91 \times 10^{-3} (0.4)^{1/2} = 4.38 \times 10^{-3} \text{ cm}$$

$$= 43.8 \text{ micron}$$

For V_a = 80 volts

$$W = 6.91 \times 10^{-3} (80)^{1/2} = 62 \times 10^{-3} = 620 \text{ microns}$$

$$E_{max} = .042 \times 10^{6} \times 6.2 \times 10^{-2} = .26 \times 10^{4} \text{ v/cm}$$

$$= 2.6 \times 10^{3} \text{ v/cm}$$

$$\Delta W = 620 - 44 = 576 \times 10^{-4} \text{ cm} = 5.76 \times 10^{-2} \text{ cm}$$

P^+-N Heterojunction

For a P^+-N heterojunction, i.e., $N_{A1} >> N_{D2}$

$$W = \left[\frac{2\varepsilon_2}{qN_{D2}}\right]^{1/2} \left[(V_b - V_a)\right]^{1/2}$$

$$E_{max} = \frac{qN_{D2}}{\varepsilon_2} W$$

where V_b = 0.6 volt (2)

For V_a = 0,

$$W = 6.91 \times 10^{-5} (0.6)^{1/2} = .537 \text{ micron}$$

$$E_{max} = .042 \times 10^{10} W = .042 \times 10^{10} \times .537 \times 10^{-4}$$
$$= .0225 \times 10^{6} = 2.25 \times 10^{4} \text{ v/cm}$$

For V_a = -10 volts

$$W = 6.91 \times 10^{-5} (10.6)^{1/2} = 2.25 \text{ microns}$$

$$E_{max} = .042 \times 10^{10} W = .042 \times 10^{10} \times 2.25 \times 10^{-4}$$
$$= 9.5 \times 10^{4} \text{ V/cm}$$

then

$$\Delta W = 2.25 - .54 = 1.71 \text{ micron}$$

APPENDIX III

Calculations of Temperature Rise in Diodes

(1) MIS

$$\text{Power} = \frac{.5 \times 10^{-3} \times 4}{2} = 1 \text{ mW}$$

$$\text{Volume } .01 \text{ in}^2 \times (2.54)^2 \times .78 \times 10^{-4} = 5 \times 10^{6} \text{ cm}^3$$

$$T = \frac{P\tau}{CpV}$$

where Cp = 1.8 joule/deg -cc

τ = period of square wave

Inserting these values

$$\Delta T = \frac{10^{-3} \times 2.5 \times 10^{-3}}{1.8 \times 10^{-6} \times 52} = .277°C \text{ per cycle}$$

But for CdS

$$Eg = 1 \text{ Å/deg. C}$$

So the change in the energy gap is small, even at this value of current.

(2) Schottky Barrier Diode

For 10Ω -cm CdS,

$$\text{Power} = P = \frac{4 \times 50 \times 10^{-6}}{2} = 10^{-4} \text{ watt}$$

$$\text{Volume} = \pi \frac{(.075 \times 2.54)^2}{4} \times 1.5 \times 10^{-4} = 4.15 \times 10^{-6} \text{ cm}^3$$

$$\Delta T = \frac{10^{-4} \times 2.5 \times 10^{-3}}{1.8 \times 4.25 \times 10^{-6}} = .0326°C \text{ per cycle}$$

For high resistivity CdS

$$P = \frac{80 \times 50 \times 10^{-6}}{2} = 2 \times 10^{-3} \text{ watt}$$

Volume = 2.83×10^{-6} t where t is in microns

$= 2.83 \times 10^{-6} \times 620 = 1758 \times 10^{-6} = 1.758 \times 10^{-3}$ cm^3

$$\Delta T = \frac{2 \times 10^{-3} \times 2.5 \times 10^{-3}}{1.8 \times 1.758 \times 10^{-3}} = 1.58 \times 10^{-3} = .0016°C \text{ per cycle}$$

(3) P^+-N Heterojunctions

$$P = \frac{10 \times 4 \times 10^{-6}}{2} = 20 \times 10^{-6} = .02 \text{ mW}$$

Volume = 2.83×10^{-6} t = 2.83×10^{-6} (1.5) - 4.25×10^{-6} cm^3

$$\Delta T = \frac{P\tau}{CpV} = \frac{.02 \times 10^{-3} \times 2.5 \times 10^{-3}}{1.8 \times 4.25 \times 10^{-6}} = .0065°C \text{ per cycle}$$

For all cases the rise in temperature per cycle is very small if the differential method is used. With d-c biases more care must be taken in mounting the samples to provide heat sinks.